Ore Geology Reviews 111 (2019) 102984

Contents lists available at ScienceDirect

Ore Geology Reviews

journal homepage: www.elsevier.com/locate/oregeorev

Mineralogy, geochemistry, and fluid action process of uranium deposits in the Zhiluo Formation, Ordos Basin, China

Qiang Zhu[a,b,*], Reng'an Yu[a,b], Xiaoxi Feng[a,b], Jianguo Li[a,b], Xianzhang Sima[a,b], Chao Tang[a,b], Zenglian Xu[a,b], Xiaoxue Liu[a,b], Qinghong Si[a,b], Guangyao Li[a,b], Sibo Wen[a,b]

[a] Tianjin Center, China Geological Survey, Tianjin 300170, China
[b] Laboratory of Non-Fossil Energy Minerals, Tianjin Center of China Geological Survey, Tianjin 300170, China

ARTICLE INFO

Keywords:
Altered minerals
Major elements
REE
Water-rock evolution
Zhiluo Formation
Ordos Basin

ABSTRACT

Some controversies still exist regarding the genesis of sandstone-type uranium deposits in the northeastern Ordos Basin. Herein, based on boreholes and well logging data, we selected sandstone samples representing different epigenetic alteration environments as the research object and comprehensively utilized polarizing microscopy, scanning electron microscopy, electron probe analysis, elemental analysis, and other test methods to research sandstone genesis. The main altered minerals in the sandstone of this area include limonite, pyrite, achavalite, carbonate, sulfate, clay, and uranium minerals. The complex characteristics of alteration minerals indicate multi-stage fluid mixed mineralization in this area. According to the relationship between the major elements in different types of sand bodies, the components were classified into three groups. The first is the reduction media group, including CaO, MnO, total oxygen carbon (TOC), S, U, and burning loss. The second is the detrital particle group, including SiO_2, K_2O, and Na_2O, and the third contains the clay and volcano component group, including Fe_2O_3, P_2O_5, TiO_2, FeO, MgO, and Al_2O_3. Among these, the content of reduction media is positively correlated with uranium enrichment, whereas detrital particles and clay components reflect the influence of alteration on the sand body composition, which indirectly affects the uranium adsorption and precipitation. Through the normalization of rare earth element (REE) chondrites, we find that the distribution patterns of REEs in rocks with different geochemical environments show a fractionation of light and heavy rare earth elements (HREEs), a right-leaning enrichment of light rare earth elements (LREEs), and relatively flat HREE. Further, via the Post Archean Australian Shale (PAAS) normalization, we observe that the mudstone of the Zhiluo Formation exhibits a relatively flat curve, whereas the sandstones have strongly positive Eu anomalies. The difference in REE values for different types of sand bodies indicates that, although all types of rocks have a similar sedimentary environment, their original sediments underwent fluid alterations such as oxidation and reduction. Based on the uranium mineralization evolution history in the study area, the water-rock reaction process and mineral-alteration sequence were determined on the basis of alteration types and elemental concentrations. Our findings provide new insight into the petrological significance, mineralogy, and geochemical composition of uranium deposits in the Ordos Basin.

1. Introduction

Sandstone-type uranium is an important type of uranium resource with great potential in northern China. Since the beginning of the 1990s, China has made substantial efforts to explore sandstone-type uranium deposits and has successively established three large sandstone-type uranium deposit bases in the Yili, Tuha, and Ordos Basins. Several studies on metallogenic regularity and metallogenesis of sandstone-type uranium deposits or uranium orefields have been conducted in the Yili, Tuha, Ordos, Erlian, and Junggan basins (Quan and Li, 2002; Wu et al., 2003; Wei et al., 2006; Li et al., 2008; Feng et al., 2014; Bonnetti et al., 2014; Jin et al., 2016). Furthermore, a uranium metallogenic model called “multi-stage uranium mineralization” has been established to explain the interlayer oxidation zone sandstone uranium deposits in continental basins of China; this model reveals the metallogenic mechanism to be a combination of paleoclimate, tectonic events, uranium-bearing rock series, oxidizing fluids, oil and gas reduction, thermal reform, and other factors (Chen et al., 1997; Jiao et al., 2004, 2005; Huang and Li, 2007; Xue et al., 2010a; Min et al., 2005; Jin et al., 2014a; Cheng et al., 2018, 2019). Jin et al (2014b)

* Corresponding author at: Tianjin Center, China Geological Survey, Tianjin 300170, China.
E-mail address: zhuq1987@163.com (Q. Zhu).

https://doi.org/10.1016/j.oregeorev.2019.102984
Received 8 May 2018; Received in revised form 6 June 2019; Accepted 17 June 2019
Available online 18 June 2019
0169-1368/

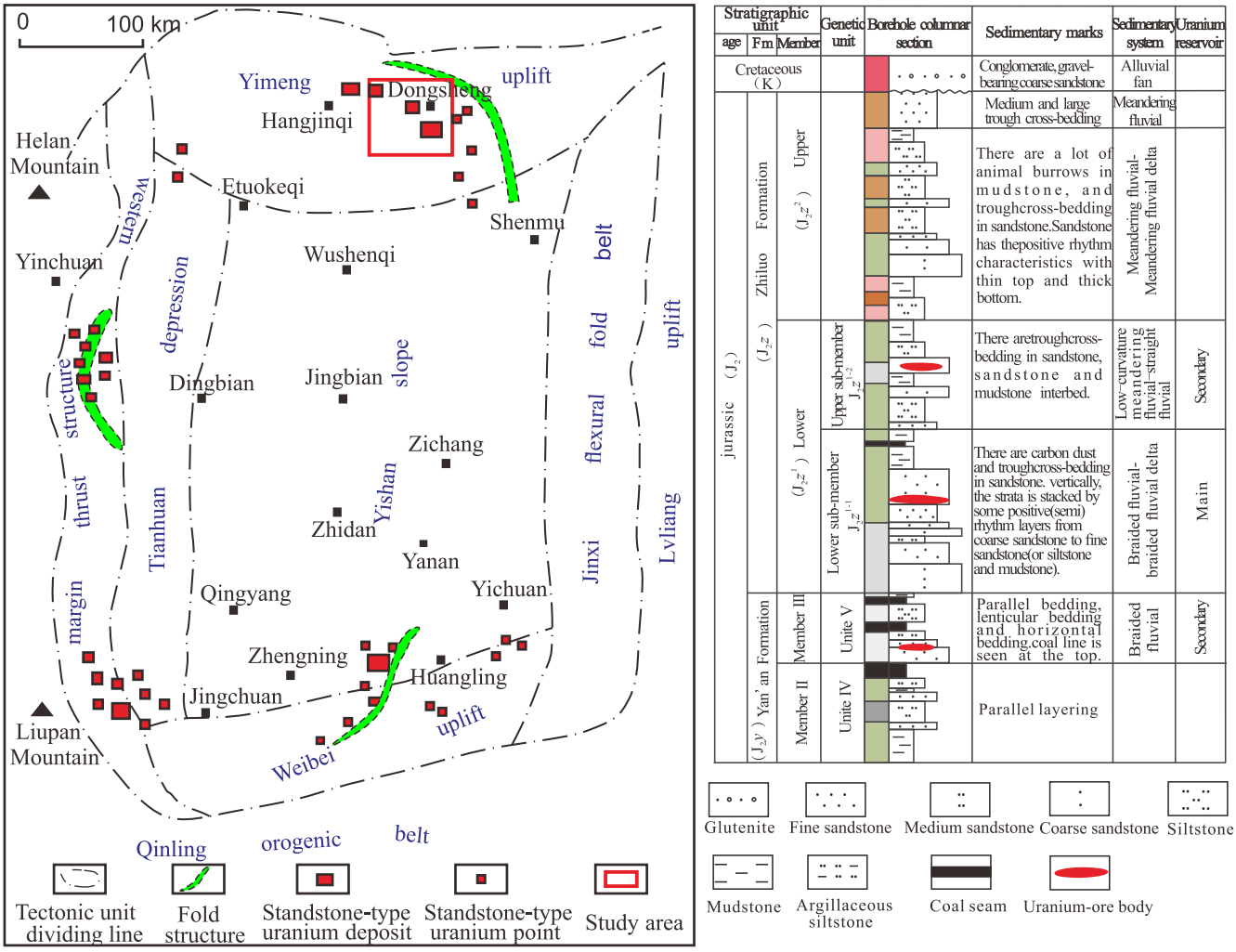

Fig. 1. Structure-outline map of the Ordos Basin and a composite columnar section of the study area.

proposed a classification scheme of typical uranium deposits based on the geological role of uranium mineralization.

The Ordos Basin possesses various energy resources such as oil, gas, coal, and uranium. In particular, abundant sandstone-type uranium deposits exist in the northeastern part of the Ordos Basin; large and medium-sized uranium deposits such as Zaohuohao, Nalinggou, and Hantaimiao have been discovered. Recently, in addition to the idea of combining coal and uranium for energetic applications and following the discovery of an ultra-large sandstone-type uranium deposit in the Daying area, increasing efforts have been made to research the occurrence mechanism of the uranium deposit in the Ordos Basin. Consequently, the northeastern region has again become a hot spot for the exploration and research of sandstone-type uranium deposits. Many achievements have been made in research involving sedimentary systems, hydrological conditions, metallogenic conditions, metallogenic mechanisms, hydrocarbon alteration, and types of uranium mineral assemblage (Zhang et al., 2017, 2005; Xiang et al., 2006; Li and Li, 2011). However, the process of fluid action in mineralization has always been controversial. Elemental analysis of sand bodies in the Dongsheng area by Luo et al. (2005) studied the type of diagenesis and the composition of the altered minerals. They discovered that the formation of uranium sandstones is mainly related to the migration of natural gas. Pan et al. (2007) proposed that gray sandstone and ore-bearing sandstones have the same combination of ore-forming elements and rare earth elements (REEs). The grayish–white kaolinized argillaceous siltstone is formed in an oxidizing environment, and gray–green coarse sandstones have experienced thermal fluid reduction from deep strata. Xiao et al. (2004a), Zhang et al. (2006), and Xue et al. (2010a) further hypothesized that oxidizing and reducing fluids jointly control the character of the Dongsheng ore deposit. They found that the altered minerals exhibit multi-stage characteristics; the mineral combination in the Dongsheng ore deposit is complex and the ore-forming fluids are low-temperature hydrothermal solutions (70 °C–120 °C). Yang et al. (2008) and Wu et al. (2013) proposed that there is a significant correlation in this area between U and some trace elements, such as Th, V, Mo, Zr, Pb, Ti, and Au. The sedimentary strata are subjected to magmatic hydrothermal action from deep strata, thus promoting the migration of organic matter and resulting in secondary enrichment of the uranium deposits. Zhu et al. (2003) discovered that the combination of trace elements found in ore-bearing sandstones in the Dongsheng area have both exogenous and deep-source properties. They suggested that deep fluids or coalbed methane, in either oil or gaseous form, participate in the mineralization of sandstone-type uranium deposits. Wu et al. (2006, 2016) presented different opinions on this issue and believed that the main source of reducing fluid was actually coal-derived gas and a small amount of oil and gas. They also believed that the mineralized uranium had experienced the action of low-temperature hydrothermal solutions and was independent of deep hydrothermal fluids. Cao et al. (2016) established a unifying model for uranium mineralization based on the results of petrology, inclusions, and isotopes, wherein early coupled bacterial uranium mineralization and hydrocarbon oxidation are followed by recrystallization of ore phases in association with low-

temperature hydrothermal solutions under hydrocarbon-induced reducing conditions.

The extensive existing literature evidences that some consensus has been reached on the understanding of uranium mineralization in the Northeastern basin. However, only few in-depth studies exist on some key scientific issues, such as the epigenetic alteration characteristics of different types of sand bodies, the causes of alteration, and the geochemical indicators related to uranium mineralization. In addition, there is no systematic analysis of the source of the fluid, which stage in the uranium mineralization process the fluid acts on, and the corresponding mineral composition changes at each stage. In this context, based on extensive literature research, detailed field investigation, and systematic analysis and research in the northeastern part of the basin, we select the drilling cores of areas with good metallogenic conditions, such as Tarangaole, Nalinggou, and Daying (called "study area" in the remaining part of the manuscript) to perform macroscopic observation and related analyses. In addition, we study the petrological significance, mineralogical alteration, and geochemical characteristics of sandstones and their relationship with uranium mineralization to provide mineralogical and geochemical constraints for this genesis study of uranium deposits; finally, we establish the stage mode of fluid action in uranium mineralization

2. Regional geological background

Located in the northwestern part of the North China Plate, the Ordos Basin is a multi-cycle craton superimposed basin having an area of $\sim 25 \times 10^4\,km^2$. It presents North–South oriented rectangular distribution: this basin is located near the Qinling orogenic belt in the South and extends to the Yimeng uplift in the North; it is adjacent to the Helan Mountain and the Liupan Mountain in the west; and it is separated from the Lvliang uplift by the Jinxi flexural fold belt (Figs. 1 and 2) (Deng et al., 2005a,b; Hou et al., 2017). The Ordos Basin is a large depression basin developed during the Mesozoic with the characteristics of overall uplift, continuous subsidence, gentle slope, low uplift, and complete stratum. The anticline in the basin is rare, the sedimentary cover is thin, and the magmatic activity is weak. (Darby et al., 2001; Davis et al., 2002).

The cap rocks of the Ordos Basin are composed of the Middle and Upper Proterozoic, Paleozoic, Mesozoic, and Cenozoic rocks, whereas Lower Carboniferous, Devonian, and Silurian rocks are missing. The strata differ in horizontal and vertical development. The Triassic, Jurassic, and lower Cretaceous constitute the main body of sedimentary cover in the basin.

This study aims to analyze the characteristics of the sandstones in the Zhiluo Formation strata (section) in the Ordos Basin. The Zhiluo Formation in the study area was in contact with the lower Cretaceous Zhidan Group (K_1zh) in the overlying Cretaceous and underlying Yan'an Formation ($J_{1-2}y$). According to the characteristics of the paleoclimate during the depositional period, the Zhiluo Formation can be divided into a lower and an upper member. The upper member of the Zhiluo Formation is a set of red clastic rock associations, where the sand body is relatively undeveloped. The lower member of the Zhiluo Formation is dominated by gray and gray-green clastic rocks. According to the sedimentary system analysis, the upper member of the Zhiluo Formation comprises the meandering river and meandering-river delta sediments. The lower member of the Zhiluo Formation is further divided into braided river sediments in the lower sub-member and braided river low-curvature meandering-river transition sediments in the upper sub-member (Figs. 3 and 4). The sedimentary sand bodies in the channel of the lower member of the Zhiluo Formation are rich in organic matter, pyrite, and other reducing media (Fig. 5a).

3. Samples

Herein, 63 samples were taken from the Jurassic Zhiluo Formation in the drilled target stratum of uranium mineralization at the Tarangaole and Nalinggou areas in the northeastern basin. These samples represent different geochemical environments and include calcareous, red, gray, gray-green, grayish–white, and mineralized sandstones. They were processed and analyzed in the Analytical Laboratory of Beijing Research Institute of Uranium Geology and the Lab of Non-Fossil Energy Minerals, Tianjin Geological Survey Center, China Geological Survey. The samples' major elements were analyzed via X-ray fluorescence spectrometry, a method that has an accuracy better than ± 2%, and the trace and REEs were identified using the American X series II model inductively coupled plasma-mass spectrometer (ICP-MS), that has an accuracy better than ± 5%. During data standardization, the sedimentary data of China were adopted from the Li's work (1994), the REE abundance data of chondrite meteorites were adopted from the Taylor and McLennan's work (1985), and the PAAS abundance data were adopted from McLennan's work (1989). The Ce and Eu anomalies in Table 5 were calculated using the Taylor's formula (1985), *i.e.*, $\delta Ce = CeN/(LaN \times NdN)^{1/2}$ and $\delta Eu = EuN/(SmN \times GdN)^{1/2}$, where N represents chondrite normalization.

Electron probe and energy spectrum analyses were primarily performed by the Lab of Non-Fossil Energy Minerals at the Tianjin Geological Survey Center, which is part of the China Geological Survey. The instrument used was a JXA-8100 electronic probe from JEOL Japan Electronics Co., Ltd (acceleration voltage 20 kV; beam 20nA; beam spot diameter 1 μm; emergence angle 40°). Periodic operating point (POP) analysis method was used together with the ZAF modified method.

The types and combinations of altered minerals were identified using polarized light microscopy, scanning electron microscopy (SEM), and electron probe microscopy.

Cluster and factor analyses were used to discuss the significance of the major elements' contents. The objective of cluster analysis is to establish a relationship between the sandstone components, which contributes to the analysis of the sandstones' mineral composition. Through cluster analysis, we can classify the sandstone components based on their similarities and correlation degree of their main features. Factor analysis can reorganize multiple variables according to the correlation under the premise of avoiding geological information loss to the maximum extent for generating a small number of new variables that represent geological information or "factors."

4. Alteration-mineral types and combination characteristics of the Zhiluo Formation

The sandstones of the ore-bearing target layer of the Zhiluo Formation are mainly gray–green and gray with locally visible red sandy clumps or spots. According to the classification method of Zhao and Zhu (2001), the lithology of these sandstones is lithic arkose sandstone, feldspathic lithic quartz sandstone, and a small amount of feldspathic litharenite. Clastic particles are mostly contact cementation or base cementation and the sorting grade is medium. Several types of debris can be identified in these sandstones, including quartzite, tuff, granite, trachyte, mudstone, and silty mudstone lithic fragments.

Seven types of mineral alterations have been identified in different types of sand bodies of the Zhiluo Formation in the study area: ferritization, pyritization, ferroselenium mineralization, carbonation, sulfation, clayization, and uranium mineralization.

(1) *Ferritization.* The continuous stratified distribution of red sandstones in the abovementioned section can be observed rarely. The rocks therein are mostly sandstone lenses or sandy blocks (spots) in the gray–green sandstones (Fig. 5b and c), and their composition is dominated by goethite, debris particles, and cement, which are entirely or partially impregnated (Fig. 5d and e).
(2) *Pyritization.* According to the formation period and its relationship with uranium metallogenesis, pyrite can be divided into three phases. The first phase is the early diagenetic pyrite, including

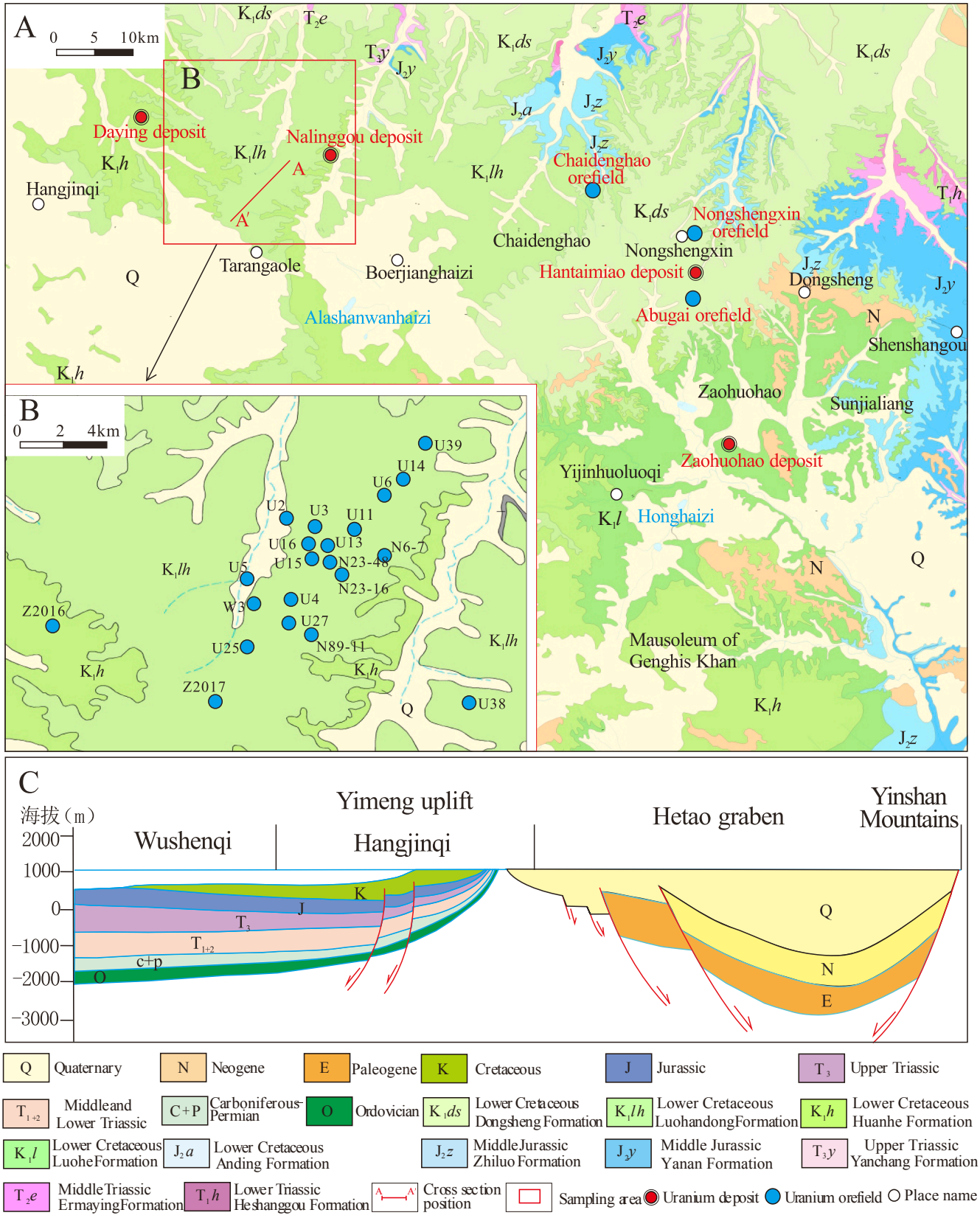

Fig. 2. A. Geological map of the northern Ordos Basin showing the locations of the study area. B. Location and numbers of the drill holes. C. Cross-section of the northern Ordos Basin.

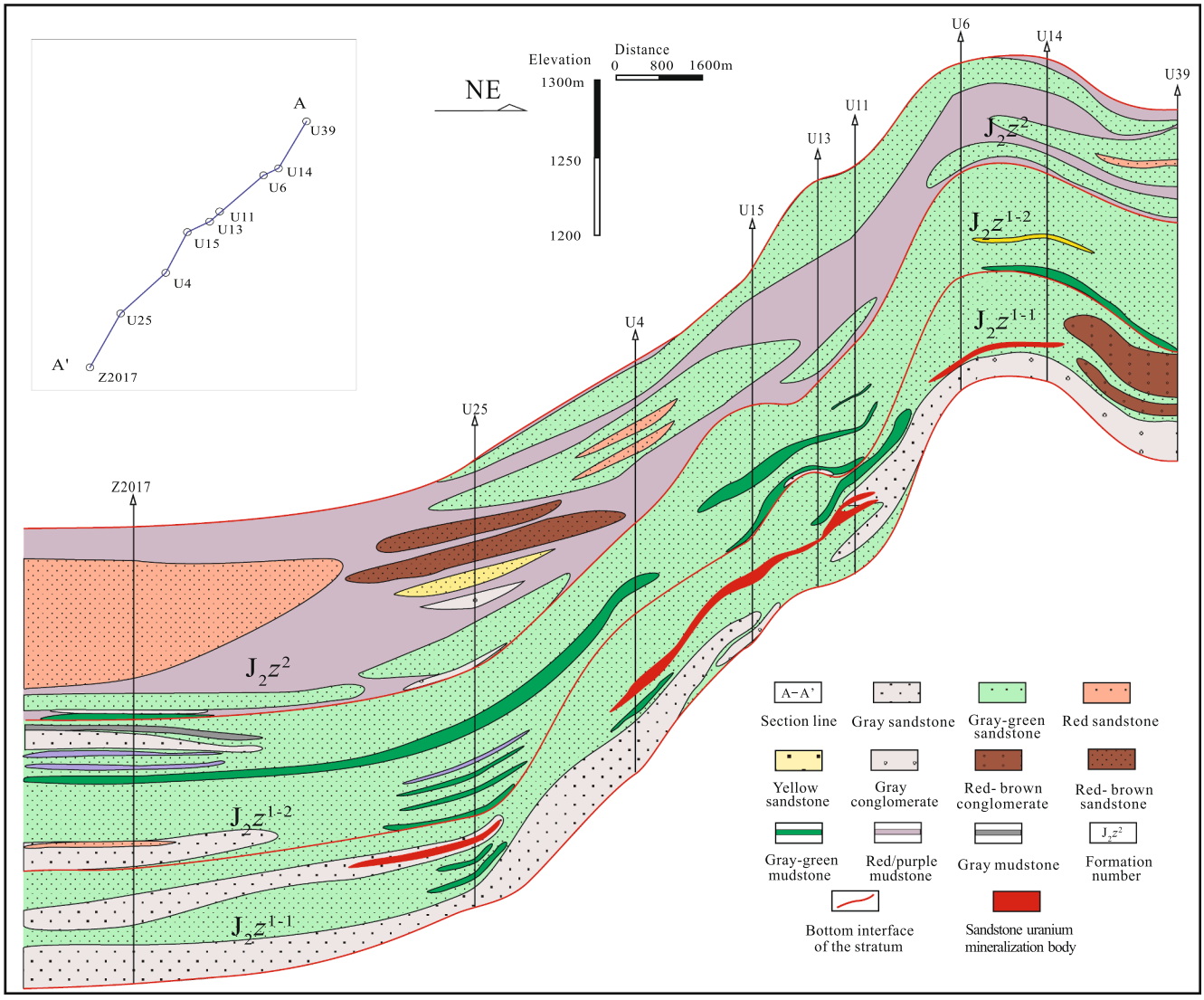

Fig. 3. The northeast–southwest (NE–SW) sandstone-type map of uranium reservoirs in the Zhiluo Foramation, TaRanGaoLe-XinSheng area, and the northeastern part of the Ordos Basin.

raspberry-like pyrite and granular pyrite (Fig. 5f). The second phase is the late diagenetic pyrite, mainly colloidal pyrite, produced in the gaps of clastic (Fig. 5g). The third phase is the pyrite in the metallogenic stage, mainly precipitated in biotite in colloidal and allotriomorphic forms, which is characterized by co-occurrence with uranium minerals (Fig. 5h).

(3) *Ferroselenium mineralization.* Achavalite was found in the sand bodies of the target strata in the Tarangaole region. It accumulates in the pores or fissures of the particles and is often associated with pyrite and other selenium minerals (Fig. 6a). SEM results show that achavalite is either a metasomatic mineral of pyrite or develops around the pyrite. Although Se can be enriched in sandstone-type uranium deposits, the results of previous studies reveal that the majority of Se and Re in sandstone-type uranium deposits occur in the form of adsorbed states. Only few sandstone-type uranium deposits contain small amounts of clausthalite, achavalite, and other independent minerals of selenium (Wang et al., 2006; Peng et al., 2006). The discovery of achavalite in the study area may indicate that the region experienced the transformation of hydrothermal fluids at low and medium temperatures (Pan et al., 2009; Zhang et al., 2015a,b).

(4) *Carbonation.* In the core, we can see the carbonate veins developed in the red calcareous sandstones in addition to the fine-crystalline calcite vein developed inside the plant charcoals in the fine gray sandstones. These observations indicate the transformation of the late-fluid effect (Fig. 6b and 6c). Carbonation, in general, can be divided into three phases. In the first phase, micritic calcite with a grain diameter of few microns was formed in the diagenesis stage (Fig. 6d). In the second phase, coarse-grained calcite with a grain diameter larger than 0.5 mm was formed with poor brightness and evident traces of recrystallization. Calcite often presents metasomatism with matrix and partial metasomatism with detritus particles. In the area where carbonation is particularly strong, the sand grains are residual (Fig. 6e), whereas locally, the sandstones retain remnants of early oxidation. The third phase of carbonation is the most advanced carbonation in the region and presents calcite veinlets or microsphygmia output commonly with two groups of complete cleavage (Fig. 6f): high brightness and high cleanness.

(5) *Sulfation.* In the study area, crumb or bedding gypsum veins can be observed in the sandstone body (Fig. 6g). Through alteration spectral scanning, we observed that gypsum cementation is widespread in the sand body. Gypsum may experience recrystallization in the later stage of fluid action such that the particles become coarse.

(6) *Clayization.* The clayization of the uranium-bearing rock series in the study area mainly includes chloritization, kaolinization, and

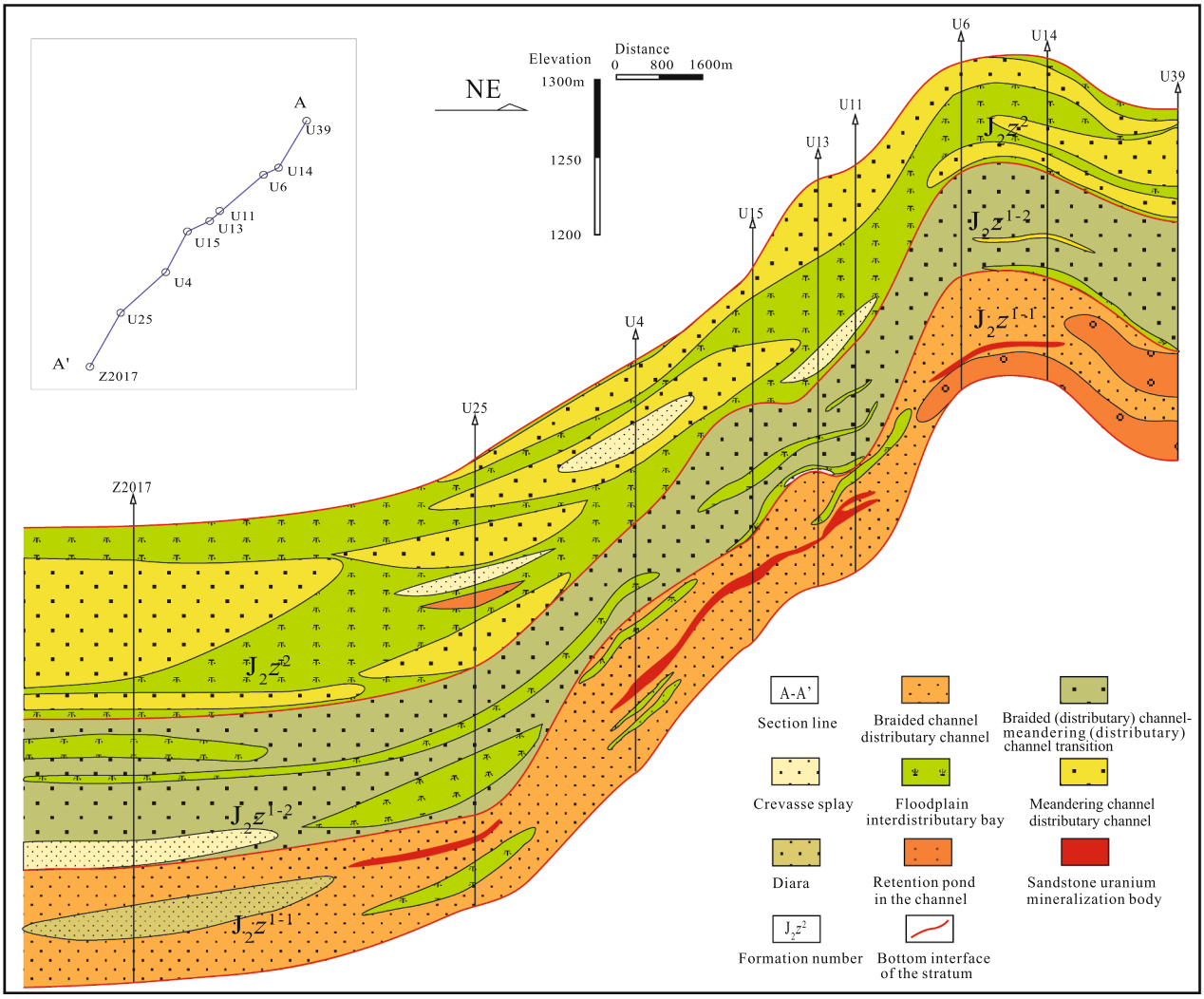

Fig. 4. The NE–SW sedimentary profile of uranium reservoirs in the Zhiluo Formation and TaRanGaoLe-XinSheng area in the Northeastern Ordos Basin.

micazation.

Chloritization of sandstones mainly includes the chloritization of biotite and chlorite rims or coatings on the surface of clastic particles. Part of the biotite was altered into pennine (Fig. 6h), which is leaf-like, light green, and presents significant pleochroism. Tiny membraniform coniferous chlorite aggregates on the surface of detritus particles could not be identified and they were present only as an extremely thin, green edge on the edge of the detritus particles (Fig. 6i).

Hydromicazation is mainly manifested as hydromicazation of plagioclase in sandstones (Fig. 6j).

Kaolinization of sandstones mainly includes kaolinization of mica (Fig. 6k) and potassium feldspar. The kaolinization of potassium feldspar is widespread, but the alteration degree is weak. Kaolinite dust, *i.e.*, dot-like kaolinite, can be seen on the feldspar surface (Fig. 6l).

(7) Uranium mineralization. Uranium primarily exists in the form of uranium minerals, adsorption uranium, and uranium-bearing minerals in the ore. Uranium minerals are mainly coffinite and a small amount of uraninite. Coffinite is mainly distributed in the following four forms. First, it appears in a colloidal form on the periphery of pyrite and detrital minerals (Fig. 7a and b). Second, it is disseminated on detritus particles (Fig. 7c). Third, it is located in the cleavage crack of biotite (Fig. 7d). Finally, coffinite metasomatism with pyrite can be observed (Fig. 7e). Adsorption uranium is mainly adsorbed by organic matter and clay minerals in rocks. Uranium-bearing minerals are symbiotic with ilmenite and leucoxene (Fig. 7f). Through electron probe analysis, the uranium associated with ilmenite has a relatively higher TiO_2 content of more than 1%, whereas uranium without any obvious symbiotic relationship to ilmenite has a generally low content of 0.15%–0.6% (Table 1). Preliminary analyses indicate that during the formation of uranium-bearing minerals, ilmenite undergoes alteration processes, resulting in the precipitation of iron and enrichment of titanium along with the enrichment and precipitation of uranium. However, further analysis is required to determine whether the uranium-bearing minerals are brannerite or titanium-bearing uranium minerals.

5. Analysis of the geochemical characteristics of sandstones in the Zhiluo Formation

5.1. Multivariate statistical analysis of major elements in sandstones of the Zhiluo Formation

We conducted a multivariate statistical analysis of the elements in different types of sand bodies in the Zhiluo Formation in the study area (Table 2) to attain a deeper understanding of the meanings of element combinations in ore-bearing sandstones and attempted to determine the factors resulting in uranium enrichment.

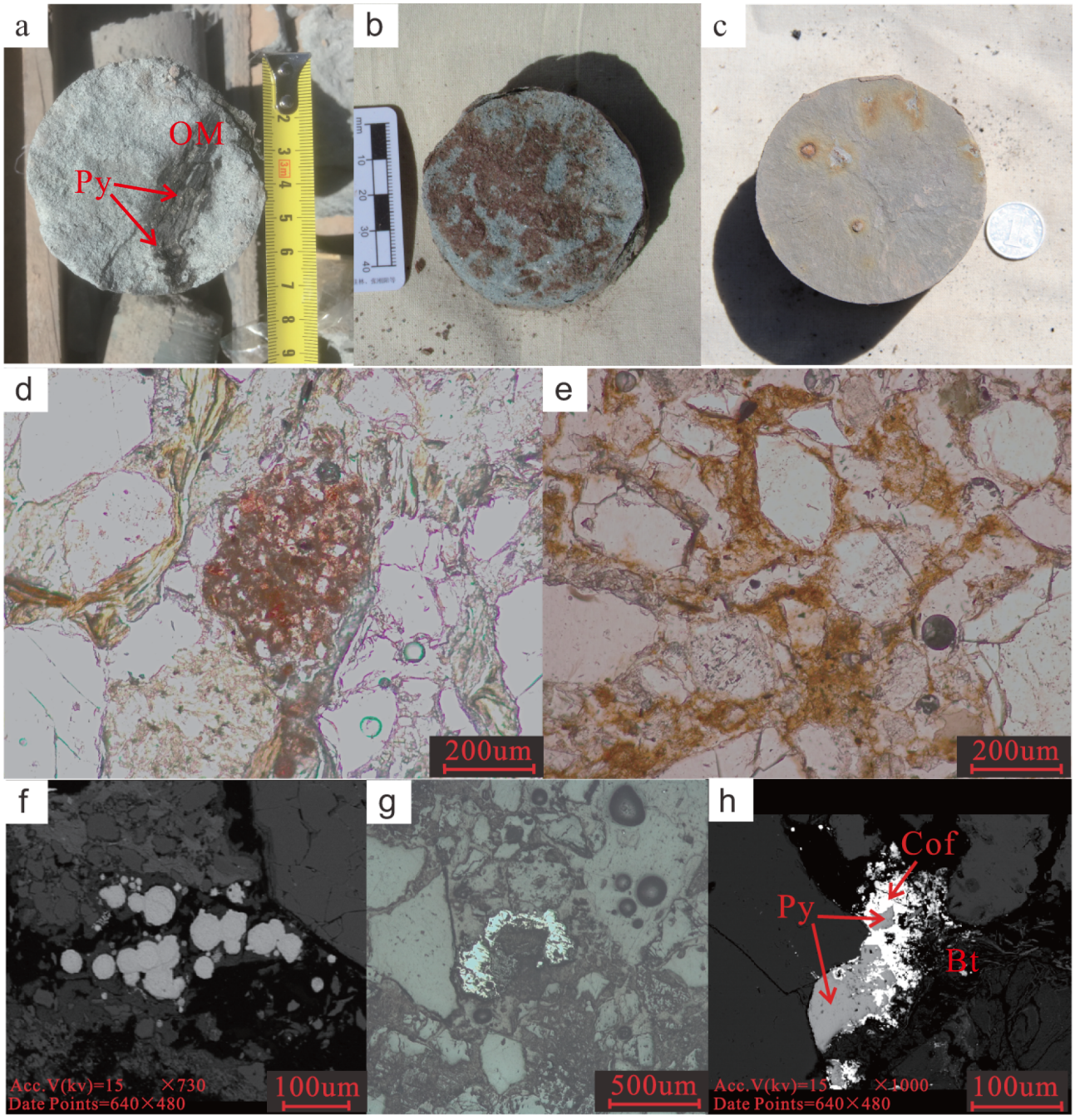

Fig. 5. Petrological characteristics of altered minerals. a) Pyrite and organic matter (carbon dust) coexist in gray sandstones; b) gray–green sandstones with red sandy lumps; c) shallow purple siltstone containing limonite nodules; d) all debris particles are brown, in plain light; e) the edge of the detritus particles is brown, plain light; f) framboidal pyrite; g) colloidal pyrite; h) pyrite associated with uranium minerals. Py: Pyrite; cof: Coffinite; OM: Organic matter; Bt: Biotite. (For interpretation of the references to color in this figure legend, the reader is referred to the web version of this article.)

5.1.1. Cluster analysis

R-type cluster analysis was conducted on the major elements and characteristic elements in sandstones of the Zhiluo Formation. A related dendrogram was obtained as follows (Fig. 8). Considering the dotted line in the hierarchical diagram as the boundary, the diagram can be divided into five subgroups and three large groups. The first group is the reduction media group, including CaO, MnO, total oxygen carbon (TOC), S, U, and burning loss. The second group is the detrital particle group, including SiO_2, K_2O, and Na_2O. The third group is the clay and volcano component group, including Fe_2O_3, P_2O_5, TiO_2, FeO, MgO, and Al_2O_3.

In the R-type cluster analysis, CaO, TOC, and S represent the calcite, gypsum, pyrite, plant debris, and other media primarily related to uranium mineralization, whereas SiO_2 represents major debris particle components, such as quartz, feldspar, and argillaceous cement. Fe_2O_3 and TiO_2 represent clay minerals, volcanic rocks (cuttings and interstitial matter), and other components.

5.1.2. Factor analysis

Herein, four factors were selected to represent the major and characteristic elements in the sandstones. In the R-factor analysis adopted above, the cumulative variance contribution rate reached 90%. Table 3 lists the matrices that were rotated using the most commonly used maximum variance method for orthogonal factor rotation. The

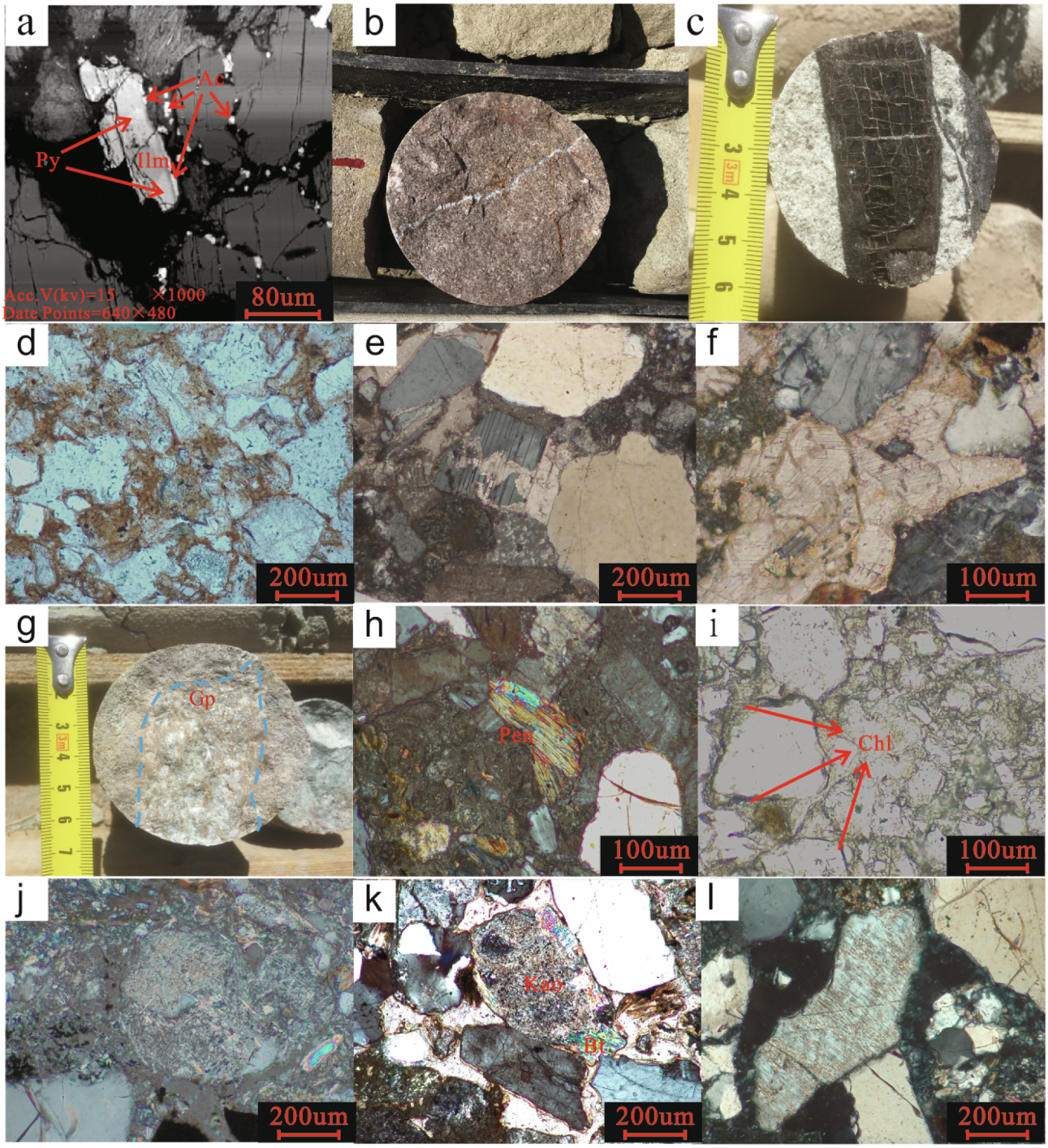

Fig. 6. Petrological characteristics of altered minerals a) Achavalite is associated with pyrite; b) red calcareous sandstones contain carbonate strips; c) a fine grid-like calcite vein can be observed in the carbon dust showing the transformation of the late-fluid action; d) mud crystal calcite, plain light; e) coarse crystal calcite, crossed Nicol; f) sparry calcite, crossed Nicol; g) fine gypsum veins grown in the green–gray sandstones; h) biotite alteration, crossed Nicol, 10 × 10; i) chlorite film on the edge of the debris particles, plain light; j) feldspar alteration into hydromuscovite, crossed Nicol; k) biotite changing to kaolinite, crossed Nicol; l) feldspar changing to kaolinite, crossed Nicol. Kao: kaolinite; Bt: Biotite; Pen: Pennine; Ac: Achavalite; Py: Pyrite; Gp: Gypsum. (For interpretation of the references to color in this figure legend, the reader is referred to the web version of this article.)

combination of elements determined via factor analysis is consistent with the cluster analysis results. The combination of minerals can thus be determined according to the load value and positive and negative symbols of the elements on the factors.

The variance contribution of the main factor F1 is 52.93%. Factor F1 represents SiO_2, Al_2O_3, K_2O, CaO, MnO, burning loss, and CO_2. SiO_2, Al_2O_3, K_2O, and Na_2O represent feldspar, quartz, and other detritus particles; further, CO_2, S, and other elements represent the inorganic components, and TOC represents the organic components. Therefore, the main factor F1 represents terrestrial detrital, cement, and inorganic matter; higher dissolution of quartz and feldspar can be observed under the microscope when calcareous cementation is strong (Fig. 6e). The dissolution of quartz indicates that the participating fluid is alkaline. In this environment, biotite is converted to chlorite, rock debris is converted into montmorillonite, feldspar is converted to montmorillonite and chlorite, and Ca, Fe, and Mg are simultaneously generated (Tang

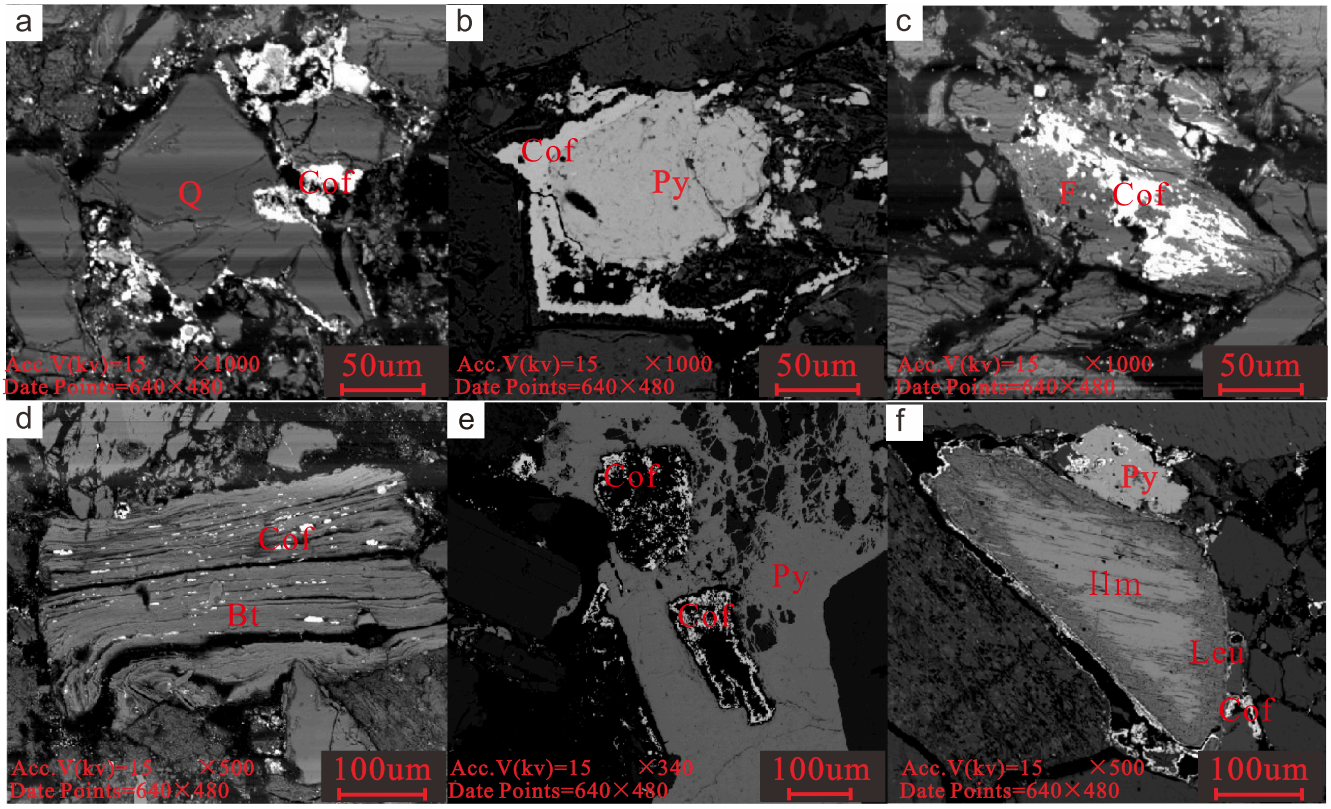

Fig. 7. Electron-microprobe backscattering images of uranium minerals. a) Coffinite distributed on the edge of quartz particles; b) coffinite distributed on the edge of pyrite; c) coffinite disseminated on detrital particles; d) coffinite distributed in biotite cleavage; e) coffinite metasomatism for pyrite; f) uranium minerals containing titanium, associated with ilmenite and titania. Py: Pyrite; cof: Coffinite; ilm: Ilmenite; Leu: Leucoxene; Bt: Biotite; Q: Quartz; F: Feldspar.

et al., 2016; Zhao et al., 2018). The conversions of kaolinite to montmorillonite and chlorite are promoted because of which the rock turns gray–green. Further research on the content of the detrital components revealed a negative correlation between the content of feldspar and clay minerals in the surrounding rock, both in low- and high-grade ores, the present research also confirms the transformation of feldspar into clay minerals, and the consumption of organic and inorganic substances through oxidative alteration (Fig. 9). Based on previous research, the lower part of the Zhiluo Formation underwent more complete oxidation and reduction (Zhu et al., 2018). Therefore, the gray–green, grayish-–white, and red sandstone samples used herein to check the TOC and S content were taken from the lower part of the Zhiluo Formation.

The variance contribution of the main factor F2 is 18.572%. Factor F2 is positively correlated to Fe_2O_3 and TiO_2. The variance contribution of the main factor F3 is 12.399%. Factor F3 is positively correlated to FeO, Al_2O_3, and MgO, and negatively correlated to Na_2O. The main factors F2 and F3 may represent the impact of muddy detrital matrix on sandstone composition. Al_2O_3 is the main component of kaolinite and montmorillonite, whereas chlorite contains FeO and MgO; Na_2O is a component of sodium feldspar; and Fe_2O_3 and TiO_2 constitute ilmenite. Therefore, main factors F2 and F3 represent the influence of clay minerals on sandstone composition. Its relationship with uranium enrichment is not obvious, but this does not mean that clay minerals do not adsorb uranium; their relationship needs to be analyzed using other methods. For example, research has shown that clay minerals have important adsorption properties for uranium, and after examining statistics of clay mineral content in the study area, we found that uranium minerals were more enriched when feldspar alterations had a higher clay content (Table 4).

The variance contribution of the main factor F4 is 8.581%. Factor F4 is positively correlated to S, TOC, and U. Factor F4 may reflect the effect of reducing media on the sandstone composition of the target stratum. S, TOC, SiO_2, Fe_2O_3, FeO, MgO, K_2O, Na_2O, P_2O_5, U, and other elements are involved in multiple factors, indicating that there are many factors affecting these elements. Alteration causes a transition between mineral components, indicating the presence of fluids in the ore-forming stage. Uranium enrichment is most closely related to TOC and S, which proves that the reducing medium is the most important factor affecting uranium enrichment.

5.2. REE distribution characteristics and correlation of sandstones in the Zhiluo Formation

Studying the behavior of REEs in metallogenesis can help us explore the source, redox characteristics, and formation process of ore-forming materials and determine the ore-bearing potential of rocks (Wang et al., 1989). Eh changes during diagenesis are most likely to affect Ce and Eu because they exist in different oxidation states in the geological environment (Henderson et al., 1984). Because REE is insoluble, the REE content of clastic rocks is mainly controlled by the rock composition of its source area (Fleet, 1984; McLennan, 1989). In comparison, the effects of weathering and diagenesis are secondary (Rollison, 2000) because changing the geochemistry of sedimentary rocks requires a huge water/rock ratio. However, owing to the hydration and adsorption characteristics of REE and the solubility differences among rare earth complexes, separation of REE may occur during deposition (Nesbitt and Young, 1984; Wang et al., 1989). In recent years, increasing attention has been paid to low-temperature mineralization. Studies on the REE changes in sedimentation, weathering, and environmental changes conclude that REE could generate fractionation under the conditions of exogenous geological processes, low temperature, low pressure, and open system (Liu and Cheng, 1995; Tu, 1998; Yang and Li, 1999; Lu and Jiang, 1999; Shao et al., 2000; Wang et al., 2000).

The rare earths in sedimentary rocks mainly comprise three parts:

Table 1
The analysis datas of electron probe.

Sample number	Lithology and colour	Depth (m)	Na_2O	MgO	Al_2O_3	SiO_2	Y_2O_3	SO_3	UO_2	K_2O	CaO	TiO_2	Ce_2O_3	FeO	P_2O_5	Total	Type
U4-1	Gray-green medium sandstone	619	0.16	0.00	/	18.64	6.07	0.09	67.77	0.19	2.63	0.28	/	0.03	0.66	96.52	the uranium without any obvious symbiotic relationship to ilmenite
U4-3	Gray-green medium sandstone	620	0.16	0.03	/	16.12	6.21	12.01	53.83	0.15	2.70	0.22	/	5.86	0.69	97.96	
U4-4	Gray-green medium sandstone	624	0.03	0.00	/	15.98	2.49	0.11	72.12	0.23	1.70	0.43	/	0.65	0.22	93.95	
U4-5	Gray-green fine sandstone	625	0.25	0.00	/	17.14	6.49	12.17	55.31	0.17	2.45	0.19	/	4.82	0.73	99.72	
U13-1	Gray-green medium sandstone	506	0.14	0.17	/	18.89	13.50	0.20	57.85	0.16	2.06	0.80	/	1.38	1.58	96.72	
U15-1	Gray-green medium sandstone	552	0.10	0.03	0.89	16.59	1.73	0.00	67.97	0.16	2.44	0.48	2.83	0.94	/	94.15	
U15-2	Gray-green medium sandstone	553	0.32	0.05	0.82	17.18	2.75	0.01	68.77	0.13	2.35	0.29	3.02	0.65	/	96.34	
U15-3	Gray-green medium sandstone	553	0.10	0.05	1.03	18.72	2.15	0.00	67.31	0.17	2.33	0.18	3.02	0.69	/	95.74	
U15-4	Gray-green fine sandstone	555	0.17	0.46	2.64	18.87	1.54	0.02	58.87	0.17	2.04	0.22	3.00	2.43	/	90.43	
U2-1	Gray-green medium sandstone	470	0.43	0.21	1.56	19.25	1.28	0.04	64.83	0.24	2.62	1.56	/	0.23	0.43	92.68	the uranium associated with ilmenite
U2-2	Gray-green medium sandstone	471	0.21	0.05	1.70	20.45	1.37	/	63.55	0.17	2.03	2.39	/	0.24	0.56	92.72	
U3-3	Gray-green medium sandstone	472	0.67	0.16	1.79	20.44	1.00	0.02	62.50	0.19	2.50	1.00	/	0.27	0.45	90.99	
U4-2	Gray-green medium sandstone	619	0.25	0.05	/	18.62	9.22	0.11	62.02	0.17	3.00	1.22	/	0.21	1.56	96.43	

/: This item was not detected.

the debris, the part adsorbed on clay minerals, and the carbonate and phosphate formed in the sedimentary process (Wang et al., 1989). Therefore, alteration of detrital particles, mutual transformation of clay minerals, and local enrichment of carbonate will cause regular changes in REE content.

The results of REE analyses on several types of rocks, such as mudstones and ore-bearing, grayish–white, gray calcareous, red, and gray–green sandstones, are reported in Table 5. REE patterns after normalization of chondrite and northern American shale are shown in Figs. 10 and 11.

5.2.1. Chondritic characteristics of REE

The total rare earth element (ΣREE) contents of the Zhiluo Formation ranges between 22.86 and 355.18 ppm with an average of 137.8 ppm, and its LREE/HREE value ranges between 5.76 and 18.49 with an average of 10.03. Post chondrite normalization, we found that REE distribution patterns in rocks belonging to different geochemical environments were right-leaning. The ratio La_N/Yb_N (for chondrite) ranges from 5 to 18.05 with an average of 11.23. The REE distribution patterns show fractionation of light and heavy rare earths, the right-leaning enrichment of LREEs, and moderate enrichment of HREEs (Fig. 10).

Table 6 presents the differences in the rare earth content in mudstones, red sandstones, gray ore-bearing sandstones, gray calcareous sandstones, gray–green sandstones, and grayish–white sandstones. According to the statistical analyses, the characteristics of the rare earth content in red sandstones and mudstones are similar, and the characteristics of calcareous sandstones and gray–green sandstones are similar. Grayish–white sandstones have the lowest total rare earth content and the lowest LREE/HREE ratio. Because the changing trend of the total rare earth content in sandstones of different geochemical types is similar to that of light and heavy rare earth content, these types of geologic bodies are deemed to have similar regularity, source, sedimentary environment, and tectonic setting. However, owing to the influence of oxidation and reduction fluid alteration, LREEs and HREEs are differentiated in different types of rocks. The value of ΣREE in red sandstones is higher than that in other sandstones. The LREE/HREE ratio is between gray ore-bearing sandstones and grayish–white sandstones. The difference between red sandstones and other types of sandstones does not support the conclusion that REEs are dissolved from oxidized sandstone and then deposited in reduced sandstone with the migration of metallogenic fluids. Ore-bearing sandstones are richer in REEs compared to the gray calcareous, gray–green, and grayish-–white sandstones. This may be because the environment created by the oxidation of organic matter and pyrite in the vicinity of uranium ore is acidic, which is beneficial to the erosion of REEs (Michard, 1989). REEs migrate from gray calcareous, gray–green, and gray–white sandstones and precipitate into ores that are rich in organic matter and clay minerals.

Based on the chondrite-normalized REE distribution patterns, we can see that the curve of the La-Sm section of mudstones in the Zhiluo Formation is steep, whereas the Dy-Lu section is relatively flat with a negative Eu anomaly (δEu = 0.6–0.8, with an average of 0.71), and no Ce abnormalities (δCe = 0.88–1.07, with an average of 0.97) are observed. LREEs and Eu are concentrated in ore-bearing sandstones, resulting in decreased Eu-negative (δEu = 0.95–1.3, with an average of 1.11) and Ce-negative anomalies (δCe = 0.77–0.95, with an average of 0.85). Furthermore, ore-bearing sandstones are highly reducible. Therefore, Eu readily forms soluble Eu^{2+} under these reducing conditions. However, because the transition zone is where the oxidation–reduction barrier is formed, the oxidation of metal sulfides, such as pyrite, generates a weak acid environment (Liu et al., 2008). Consequently, Eu^{2+} does not dissolve in water in the transition zone but is adsorbed by clay minerals and precipitates, resulting in the relative enrichment of Eu in the transition zone (Braum et al., 1993; Price et al., 1991; Chen et al., 2007). In calcareous sandstones, Eu presents weak

Table 2
major elements content for different types of sandstones in Zhiluo Formation, in the northeastern region of the Ordos Basin.

Sample number	Lithology and colour	Depth (m)	TOC (10–2)	S (10–2)	SiO_2 (10–2)	Al_2O_3 (10–2)	Fe_2O_3 (10–2)	FeO (10–2)	CaO (10–2)	MgO (10–2)	K_2O (10–2)	Na_2O (10–2)	TiO_2 (10–2)	P_2O_5 (10–2)	MnO (10–2)	灼失 (10–2)	CO_2 (10–2)	U (10–6)
U4-1	Gray-green medium sandstone	616.4	/	0.01	66.72	14.29	4.6	1.38	0.75	1.77	3.38	1.95	0.67	0.13	0.093	4.12	0.041	14.4
U4-2	Gray-green medium sandstone	615.4	/	0.432	71.45	12.42	0.45	2.38	1.81	1.45	3.32	1.58	0.58	0.096	0.065	4.04	0.95	1.97
U4-3	Gray fine sandstone	625.75	4.92	6.64	66.58	13.81	4.44	1.21	0.94	1.59	3.48	1.92	0.56	0.11	0.098	5.14	0.22	29
U4-4	Gray-green medium sandstone	624.7	1.18	1	56.24	10.65	0.95	1.39	12.3	1.08	2.88	1.57	0.37	0.074	0.35	12.01	9.02	166
U4-5	Gray-green medium sandstone	626.1	3.83	17.2	54	10.22	1.83	0.76	12.62	1.07	2.56	1.32	0.61	0.088	0.35	14.5	9.2	1280
U4-6	Gray-green medium sandstone	627.3	0.065	0.133	72.3	11.93	0.84	0.68	3.08	0.97	3.32	1.78	0.34	0.08	0.068	4.56	1.96	14.6
U4-7	Gray-green medium sandstone	631	1.48	1.22	56.95	9.28	0.67	0.59	13.36	0.73	2.85	1.49	0.2	0.066	0.32	13.44	10.04	100
U4-8	Gray-green medium sandstone	632.25	/	0.534	61.25	12.55	5.1	0.93	5.62	1.74	2.85	1.78	0.45	0.09	0.21	7.32	3.93	8.51
U4-9	Gray-green medium sandstone	642.3	2.23	25.8	50.4	8.67	0.96	0.84	17.88	0.78	2.18	1.4	0.36	0.078	0.48	15.86	13.03	44.4
U4-10	Gray-green medium sandstone	643.39	0.215	0.117	53.09	9.02	1.48	0.27	16.6	0.78	2.3	1.73	0.34	0.092	0.34	13.92	12.63	3.98
U16-1	Gray-green mudstone	516.22	0.115	0.024	59.27	14.4	5.63	5.33	2.08	2.72	2.7	1.14	0.61	0.14	0.12	5.28	0.93	3.58
U16-2	Grayish-white medium sandstone	521.75	/	/	74.65	12.23	1.09	1.4	1.11	1.12	3.38	1.97	0.4	0.08	0.041	2.39	0.27	0.79
U16-3	Grayish-white medium sandstone	524.9	/	0.032	73.42	12.98	1.51	1.29	0.92	1.09	3.53	2.15	0.56	0.093	0.042	2.27	0.021	24.8
U16-4	Gray-green medium sandstone	539.9	0.102	12.1	63.86	11.31	6.66	1.66	1.38	0.92	2.98	1.85	1	0.13	0.075	8	0.089	24.4
U27-1	Gray-green medium sandstone	624	/	/	69.1	14.22	1.68	2.22	0.64	2.29	3.31	2.08	0.82	0.15	0.048	3.17	0.056	4.66
U27-2	Gray-green medium sandstone	624.7	/	/	69.68	13.51	1.99	1.51	1.03	1.31	3.16	3.54	0.63	0.13	0.056	3.29	0.43	1.29
U27-3	Grayish-white medium sandstone	623.9	/	0.057	73.63	12.64	0.96	1.46	1.04	1.23	3.44	2.11	0.58	0.09	0.041	2.62	0.34	53.5
U27-4	Grayish-white medium sandstone	621.3	/	/	74.42	12.07	0.98	1.02	1.5	1	3.65	2.12	0.31	0.075	0.046	2.7	0.79	18.7
U5-1	Grayish-white medium sandstone	722.95	/	/	71.15	13.38	1.28	1.8	0.59	1.39	3.28	3.43	0.61	0.11	0.031	2.76	0.11	8.47
U5-2	Grayish-white medium sandstone	723.85	/	/	70.3	13.5	1.58	1.86	0.74	1.47	3.26	3.27	0.71	0.13	0.037	2.94	0.22	36.6
U5-3	Grayish-white medium sandstone	729.55	/	/	74.43	11.71	0.56	0.74	1.58	0.63	3.13	3.53	0.27	0.079	0.045	3.21	0.65	7.29
U5-5	Grayish-white fine sandstone	723.8	/	/	72.38	12.72	0.98	1.14	1	0.95	3.48	3.22	0.37	0.076	0.034	3.53	0.44	41.5
U5-8	Gray-green fine sandstone	724.2	/	/	67.55	13.91	2.28	1.43	1.16	1.28	3.04	3.08	0.6	0.11	0.046	5.35	0.59	75.5
U5-10	Gray-green siltstone	725	/	/	56.9	18.31	3.69	4.64	0.65	3.55	2.74	1.59	1.03	0.21	0.057	6.12	0.013	50

/: This item was not detected.

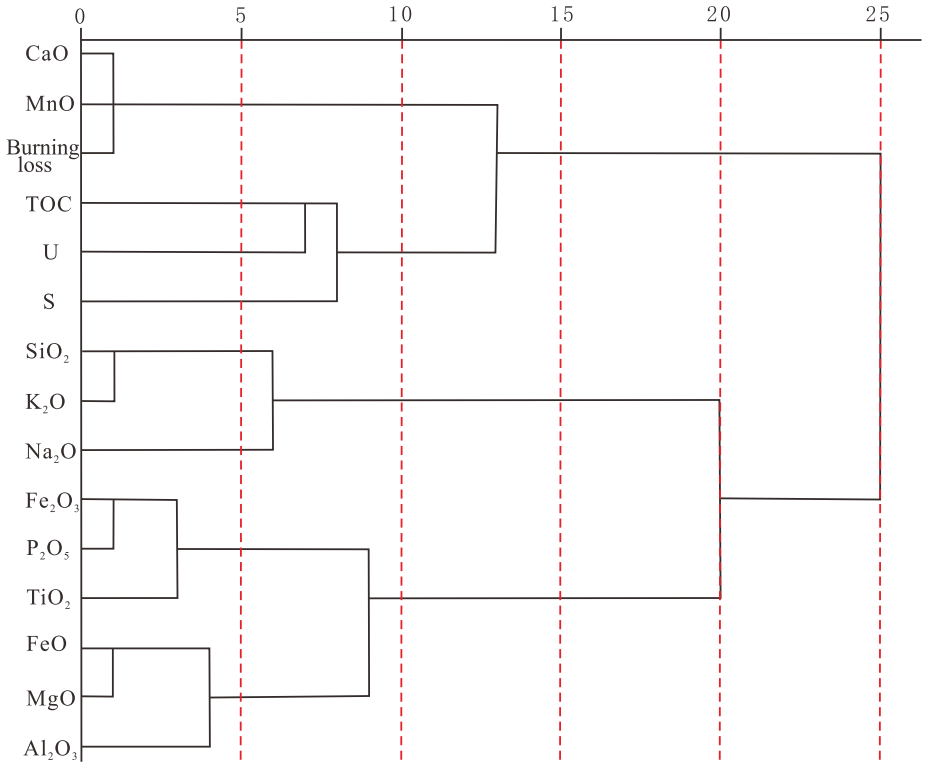

Fig. 8. Dendrogram of R-type cluster analysis.

Table 3
The varimax-factor solution matrix of uranium-bearing sandstone.

Rotating component matrix *a*				
	Component			
	F1	F2	F3	F4
S	−0.482	0.385	−0.253	0.567
TOC	0.115	−0.081	−0.069	0.898
SiO_2	0.946	0.099	−0.115	−0.144
Al_2O_3	0.751	0.301	0.569	0.020
Fe_2O_3	0.333	0.871	0.286	−0.080
FeO	0.126	0.379	0.881	−0.215
CaO	−0.847	−0.464	−0.226	0.074
MgO	0.312	0.251	0.900	−0.020
K_2O	0.971	−0.019	−0.102	0.062
Na_2O	0.546	0.115	−0.752	−0.167
TiO_2	0.185	0.947	0.027	0.134
P_2O_5	0.271	0.816	0.444	−0.149
MnO	−0.862	−0.397	−0.120	0.223
Burning loss	−0.888	−0.250	−0.278	0.218
U	−0.248	−0.017	0.062	0.789
CO_2	−0.830	−0.492	−0.225	0.068
Variance contribution rate	52.931	18.572	12.399	8.581
Cumulative variance contribution rate	52.931	71.503	83.902	92.483

negative anomalies (δEu = 0.77–0.97, with an average of 0.87), and Ce presents negative anomalies (δCe = 0.64–0.83, with an average of 0.75). In red sandstones, Eu presents a negative anomaly (δEu = 0.38–0.91, with an average of 0.64), whereas Ce either has no anomaly or weak positive anomalies (δCe = 0.98–1.61, with an average of 1.16). Eu in red sandstones exhibits the same features as those of mudstones in the study area, probably because the two have the same sedimentary and diagenetic environments (Zhu et al., 2018). In addition, oxidation may have occurred in the metallogenic period. However, as oxidation cannot cause Eu migration in sandstones, it cannot be responsible for the change in Eu content. Under the condition of high oxygen content, Ce is oxidized to Ce^{4+}. The solubility of Ce^{4+} is very low; hence, it is easily adsorbed and detached from the solution system by clay minerals, producing a weak positive Ce anomaly in minerals (Huang and Wang, 2002; Wang et al., 1989). In gray and gray–green sandstones, Eu has no anomaly or presents weak negative anomalies (δEu = 0.78–1.06, with an average of 0.92), whereas Ce presents positive and negative anomalies (δCe = 0.69–1.42, with an average of 1.0). In grayish–white sandstones, Eu presents positive anomalies (δEu = 1.24–2.49, with an average of 1.75), whereas Ce presents both positive and negative anomalies (δCe = 0.86–1.35, with an average of 1.02). The large anomalies of Ce may be due to the uneven migration and precipitation of Ce caused by the superimposed transformation of oxidation and reduction in gray–green and grayish–white sandstones. In grayish–white sandstones, the kaolinite content is significantly high as the formation of kaolinite may be related to weathering. Strong weathering will reduce the total rare earth content and the LREE/HREE ratio. The precursor mineral of kaolinite may be feldspar. The REE content of feldspar is lower than that of kaolinite, and feldspar Eu presents a positive anomaly, whereas the Eu in kaolinite presents a negative anomaly (Wang et al., 1989). Therefore, grayish–white sandstones are more likely to have experienced oxidation reactions, causing feldspar alteration and Eu enrichment via adsorption and precipitation.

5.2.2. PAAS characteristics of REE

The North American shale label (NASC) of sedimentary rocks enables us to understand the characteristics of sedimentary rocks and recognize slight enrichments and depletions of elements (Rollison, 1993; Liu, 1991). Currently, European shale (ES) and Post-Archaean average Australian sedimentary rock (PAAS) (McLennan, 1989) are usually used instead of NASC as the normalized-REE abundance of sedimentary rocks. In this study we use PAAS data for the same. From the normalized-REE distribution model (Fig. 11), we found that the mudstones of the Zhiluo Formation exhibit a relatively flat curve with an average ΣREE of 221.75 ppm. In terms of the rare earth composition, the mudstones of the Zhiluo Formation are characterized by light enrichment in rare earths and moderate Eu loss. These sandstones present

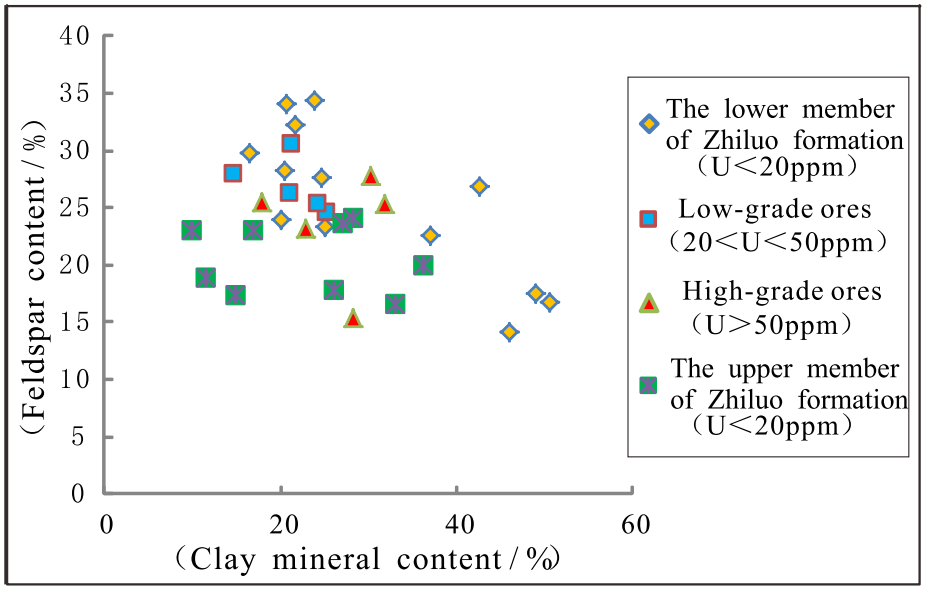

Fig. 9. Contrast diagram of feldspar and clay mineral content showing different types of sandstones.

a strong positive Eu anomaly, whereas their HREE content is not enriched as a whole. There is a slight discrepancy in the HREEs and LREEs in different types of sandstones. In particular, the LREEs and HREEs in grayish–white sandstones all exhibit an apparent loss, indicating that all types of rocks have a similar depositional environment, but they underwent oxidation and reduction transformation after the deposition period.

6. Significance of the geochemical characteristics of the uranium mineralization

Since the Paleozoic, the Ordos Basin has been uplifted. However, owing to long-term sedimentation and the formation of the Hetao fault depression, the uplift amplitude has reduced and even disappeared after entering the Mesozoic. Affected by the Yanshan's tectonic movement, when the Zhiluo Formation was deposited, the main paleogeomorphology in the northern Ordos Basin was elevated in the North and West and lowered in the South and East (Zheng et al., 2006; Han et al., 2009). In the early Yanshanian movement, the basin was fully uplifted and entered the weathering and denudation stage. The Zhiluo Formation was exposed to the surface and the oxygenated water infiltrated a large area to form oxidized sandstone. With the evolution of tectonic movement and fluid effect, the formation experienced multi-stage alteration; in particular, it later experienced reduction transformation, forming large-scale green and gray–green sandstones in the study area. Red and yellow oxide residue can still be locally observed in the sandstones, whereas the gray–green rocks retain the form of early interlayer oxidation. Therefore, the northeastern part of the basin, belonging to the ancient interlayer oxidizing zone of the sandstone-type uranium deposit, is a part of the Yinshan ancient Hetao provenance-system mineralization system (Li et al., 2008; Jiao et al., 2012).

According to the tectonic evolution history and the type of alteration and geochemical analysis in the study area, a paragenetic sequence of mineral alteration was established (Fig. 12), following which, the water-rock reaction and mineralization process was restored: from the alkaline-weak acid oxidation-fluid transition phase in the early stage to the weak acid reduction fluid phase in the middle stage, followed by the alkaline reduction fluid phase in the late stage, and the mid-low-temperature hydrothermal fluid transformation phase post mineralization (Fig. 13). This work plays a significant role in revealing the genesis of the mineralization.

6.1. Alkaline-weak acid oxidation-fluid transition phase in the early stage

Affected by the climate, the precipitation, which infiltrated the Zhiluo Formation in the Ordos Basin, was alkaline during the exposure period (Zhang et al., 2015a,b). The uranium present in the magmatic metamorphic rocks in the source area and the uranium flowing through the sedimentary formations were extracted to form oxygen-bearing uranium-rich water. After the alkaline fluid entered the target stratum, the sand body experienced oxidation, and ferritization occurred along the edge of debris particles or cracks. As the Zhiluo Formation strata contain substantial plant debris, humic organic matters oxidized to release acidic fluid (including CO_3^{2-}) during burial diagenesis, and bacteria that were possibly fed on autochthonous organic matter dispersed throughout the host sandstones to produce H_2S (Cao et al., 2016). Consequently, fluid properties changed from alkaline to weak acid (Huang et al., 2009), resulting in the dissolution of aluminosilicate minerals, such as feldspar (Huang et al., 2009), the sericitization of volcanic detritus, and the kaolinization of plagioclase. Ca^{2+} was released during feldspar alteration, which was partially involved in the precipitation of calcite in next phase. Pyrite was oxidized into goethite and sulfate (Kovačević et al., 2009). These early alterations were confirmed via SEM and electron probe microscopy.

In all types of sandstone samples, the numerical values and change rule of ΣREE, LREE, and HREE of red sandstones are closest to those of mudstone samples, whereas the content of red sandstones is much higher than that of other types of sandstones, two explanations are possible for this phenomenon. One possibility is that in the study area, the original sedimentary red sand bodies controlled by sedimentary facies are also present along with the late oxidation residue of the sand body. However, according to the second possibility, the increase in the clay content caused by the clayization and ferritization in the oxidized sand body increased ΣREE; then, the strong clayization precipitated HREEs in the secondary minerals, and, finally, HREEs moved forward along with the fluid, thus increasing the LREE/HREE ratio (Wang, 2006).

6.2. Acid reduction fluid phase in the middle stage

The reductant in study area is generally considered to be associated with the hydrocarbons migrating through the host rocks (Zhu et al., 2003; Wu et al., 2006). We suggest that these hydrocarbons represent different acidic and alkaline environments and correspond to different

Table 4
The comparison of feldspar, clay minerals and calcite in different types of sandstone.

Stratum	Rock types	Number of samples	Sample number	Lithology and colour	Depth (m)	Feldspar (%)	Clay minerals (%)	Calcite (%)
upper member of Zhiluo formation	Surrounding rocks	4	U13-31	Red medium sandstone	305.3	23	16.9	22.2
			U13-33	Red coarse sandstone	325.1	17.3	14.9	37
			Z2016-50	Red coarse sandstone	541.75	18.9	11.5	28.4
			Z2017-26	Red coarse sandstone	528.5	23.7	27	19
			Average			**20.7**	**17.75**	**26.65**
	Surrounding rocks	4	U38-17	Gray-green medium sandstone	361.2	24.1	28.2	/
			Z2016-39	Gray-green medium sandstone	462.1	17.8	26	23.9
			Z2016-48	Gray-green coarse sandstone	518.24	23	10	37.1
			Z2016-51	Gray-green medium sandstone	544.47	16.6	33	/
			Average			**20.4**	**24.3**	**15.25**
lower member of Zhiluo formation	Surrounding rocks	8	U39-17	Gray-green medium sandstone	303.5	29.8	16.4	/
			U13-55	Gray-green coarse sandstone	478.15	34.4	23.8	/
			U38-22	Grayish-white medium sandstone	441.8	27.6	24.7	/
			Z2016-69	Gray-green coarse sandstone	703.55	32.3	21.6	/
			Z2017-19	Gray-green medium sandstone	646.5	28.3	20.4	3.4
			U2-2	Gray-green medium sandstone	470.05	34.1	20.6	/
			U4-1	Gray-green medium sandstone	618.9	24	20	8.2
			U6-19	Gray-green medium sandstone	338.05	23.3	25.1	4.3
			Average			**29.2**	**21.6**	**1.59**
	Low-grade ores (U ≤ 0.01%)	4	U2-1	Grayish-white medium sandstone	471.42	26.3	21	/
			U3-3	Gray-green coarse sandstone	492.83	25.4	24.2	/
			U15-3	Gray-green medium sandstone	553.8	30.5	21.3	/
			U25-2	Grayish-white medium sandstone	617.57	24.6	25.3	/
			Average			**26.7**	**23.0**	/
	High-grade ores (U > 0.01%)	5	U2-3	Gray-green medium sandstone	477.98	25.5	17.9	/
			U3-4	Gray-green coarse sandstone	498.81	23.2	22.9	/
			U4-4	Gray-green medium sandstone	624.4	27.8	30.3	/
			U38-1	Gray medium sandstone	435.5	15.3	28.3	7.8
			U38-3	Gray-green medium sandstone	460.5	25.3	31.9	7.1
			Average			**23.42**	**26.26**	**2.98**

Table 5
REE (ppm) results for different types of sandstones in Zhiluo Formation, in the northeastern region of the Ordos Basin.

Type	Sample No.	Lithology and colour	Depth (m)	La.	Ce	Pr	Nd	Sm	Eu	Gd	Tb	Dy	Ho	Er
Mudstone	U16-1	Gray-green mudstone	516.22	37.90	65.30	8.02	30.00	5.11	1.31	4.88	0.72	3.85	0.77	2.18
	N6-7	Gray mudstone	379	52.10	97.30	12.20	47.30	8.00	1.66	6.40	1.03	5.07	0.94	2.58
	W3	Gray mudstone	507	48.40	97.50	12.10	48.50	8.92	1.97	7.61	1.32	6.78	1.27	3.37
	N89-11	Gray-green mudstone	517	53.60	102.00	11.50	42.60	7.45	1.47	6.03	0.97	4.81	0.89	2.51
	N6-7–1	Red mudstone	329	45.40	85.70	9.76	34.70	6.20	1.41	6.38	0.85	4.91	0.98	3.13
	N6-7–2	Red mudstone	329	51.10	108.00	11.00	39.70	7.50	1.73	8.96	1.47	10.30	2.30	7.20
	N23-16	Red mudstone	354	45.00	95.00	9.70	35.70	6.20	1.56	6.54	0.87	4.50	0.87	2.50
Ore-bearing sandstone	U4-4	Gray-green medium sandstone	624.7	36.60	54.40	6.91	25.00	5.26	1.64	5.30	0.85	4.97	0.94	2.50
	U4-5	Gray-green medium sandstone	626.1	45.50	138.00	27.60	111.00	11.60	3.26	8.20	0.85	3.80	0.73	2.05
	U4-7	Gray-green medium sandstone	631	28.50	44.30	5.91	22.00	4.01	1.42	3.83	0.63	3.55	0.70	1.89
	U5-8	Gray-green fine sandstone	724.20	11.10	23.00	2.92	10.90	1.97	0.76	1.97	0.31	1.78	0.35	0.98
	U27-3	Grayish-white medium sandstone	623.9	9.76	17.10	2.78	10.80	1.99	0.78	1.69	0.25	1.36	0.27	0.76
Calcareous sandstone	U4-1	Gray-green medium sandstone	616.4	34.40	48.90	8.04	29.00	4.63	1.01	3.45	0.49	2.49	0.48	1.40
	U4-2	Gray-green medium sandstone	615.4	35.10	57.00	7.34	25.90	4.12	1.11	3.37	0.49	2.60	0.50	1.44
	U4-3	Gray fine sandstone	625.75	29.60	37.80	6.38	21.80	3.15	0.79	2.63	0.36	1.86	0.38	1.10
	U4-10	Gray-green medium sandstone	643.39	30.30	47.00	6.02	21.90	3.62	1.09	3.27	0.46	2.41	0.48	1.30
Red sandstone	U3-1	Red medium sandstone	301.5	18.20	61.70	4.41	17.90	3.44	1.05	3.58	0.43	2.36	0.47	1.45
	U3-2	Red medium sandstone	320	47.00	95.90	11.30	43.80	7.54	1.66	7.16	0.82	4.09	0.70	2.07
	N23-48–1	Red fine sandstone	383	66.00	133.00	14.75	55.35	9.78	1.86	10.20	1.33	6.60	1.20	3.50
	N23-48–2	Red medium sandstone	384	37.00	84.00	9.80	35.49	7.78	0.99	7.96	1.28	7.70	1.56	4.70
Grayish-white sandstone	U5-1	Grayish-white medium sandstone	722.95	5.25	12.10	1.45	5.67	1.07	0.55	0.95	0.14	0.78	0.15	0.45
	U5-2	Grayish-white medium sandstone	723.85	8.99	23.80	2.49	9.76	1.77	0.67	1.54	0.22	1.21	0.23	0.67
	U5-3	Grayish-white medium sandstone	729.55	3.60	10.50	0.92	3.84	0.85	0.62	0.68	0.10	0.62	0.13	0.39
	U5-5	Grayish-white fine sandstone	723.8	6.14	12.10	1.65	6.33	1.18	0.70	1.09	0.19	1.19	0.24	0.72
	U27-4	Grayish-white medium sandstone	621.3	6.61	14.10	1.83	7.39	1.48	0.79	1.24	0.20	1.13	0.22	0.62
	U16-2	Grayish-white medium sandstone	521.75	8.51	16.60	2.31	8.97	1.66	0.81	1.42	0.20	1.14	0.22	0.63
	U16-3	Grayish-white medium sandstone	524.9	7.83	15.10	2.16	8.25	1.52	0.73	1.34	0.19	1.13	0.23	0.64
	U4-6	Gray-greenmedium sandstone	627.3	21.00	32.80	4.76	17.30	2.82	0.88	2.28	0.32	1.60	0.31	0.86
Gray-greensandstone	U4-8	Gray-green medium sandstone	632.25	42.20	55.60	8.55	30.40	4.94	1.29	3.99	0.56	2.88	0.56	1.63
	U4-9	Gray-green medium sandstone	642.3	33.20	54.10	7.10	26.40	4.16	1.26	3.71	0.50	2.62	0.52	1.39
	U16-4	Gray-green medium sandstone	539.9	24.00	67.10	5.83	22.10	3.81	0.99	3.55	0.52	2.88	0.57	1.66
	U27-1	Gray-green medium sandstone	624	14.80	41.20	3.13	11.40	1.81	0.46	1.80	0.23	1.14	0.22	0.72
	U27-2	Gray-green medium sandstone	624.7	11.10	25.60	3.34	13.40	2.55	0.77	2.09	0.31	1.55	0.30	0.91

Type	Tm	Yb	Lu	Y	ΣREE	LREE	HREE	LREE/HREE	Chondrite-normalized			PAAS-normalized		
									LaN/YbN	δEu	δCe	LaN/YbN	δEu	δCe
Mudstone	0.34	2.26	0.35	19.60	162.99	147.64	15.35	9.62	11.33	0.80	0.88	1.24	1.24	0.86
	0.43	2.67	0.38	26.90	238.07	218.56	19.51	11.20	13.19	0.71	0.90	1.44	1.09	0.89
	0.53	3.17	0.46	37.20	241.89	217.39	24.50	8.87	10.32	0.73	0.94	1.13	1.13	0.93
	0.42	2.68	0.39	23.30	237.31	218.62	18.69	11.70	13.51	0.67	0.96	1.48	1.03	0.95
	0.46	3.27	0.49	29.80	203.63	183.17	20.46	8.95	9.38	0.69	0.95	1.02	1.06	0.94
	0.98	5.96	0.89	98.30	257.09	219.03	38.06	5.76	5.79	0.64	1.07	0.63	0.99	1.05
	0.34	2.20	0.32	24.00	211.30	193.16	18.14	10.65	13.82	0.75	1.07	1.51	1.15	1.05

(*continued on next page*)

Table 5 (*continued*)

Type	Tm	Yb	Lu	Y	ΣREE	LREE	HREE	LREE/HREE	Chondrite-normalized			PAAS-normalized		
									LaN/YbN	δEu	δCe	LaN/YbN	δEu	δCe
Ore-bearing sandstone	0.34	2.01	0.29	24.40	147.01	129.81	17.20	7.55	12.30	0.95	0.80	1.34	1.46	0.79
	0.30	1.97	0.32	31.70	355.18	336.96	18.22	18.49	15.61	1.02	0.91	1.71	1.57	0.90
	0.25	1.50	0.22	20.60	118.71	106.14	12.57	8.44	12.84	1.11	0.80	1.40	1.71	0.79
	0.15	0.99	0.16	10.30	57.34	50.65	6.69	7.57	7.58	1.18	0.95	0.83	1.82	0.93
	0.12	0.83	0.13	5.99	48.62	43.21	5.41	7.99	7.95	1.30	0.77	0.87	2.00	0.76
Calcareous sandstone	0.22	1.52	0.25	11.60	136.28	125.98	10.30	12.23	15.29	0.77	0.69	15.29	0.77	0.69
	0.22	1.52	0.24	12.40	140.95	130.57	10.38	12.58	15.60	0.91	0.83	15.60	0.91	0.83
	0.18	1.18	0.18	9.45	107.39	99.52	7.87	12.65	16.95	0.84	0.64	16.95	0.84	0.64
	0.18	1.14	0.19	14.40	119.36	109.93	9.43	11.66	17.96	0.97	0.82	17.96	0.97	0.82
Red sandstone	0.19	1.23	0.18	15.80	116.60	106.70	9.90	10.78	10.00	0.91	1.61	10.00	0.91	1.61
	0.27	1.76	0.25	21.80	224.32	207.20	17.12	12.11	18.05	0.69	0.98	18.05	0.69	0.98
	0.48	3.32	0.50	28.99	307.87	280.74	27.13	10.35	13.43	0.57	1.00	13.43	0.57	1.00
	0.69	4.36	0.62	44.96	203.93	175.06	28.87	6.06	5.73	0.38	1.03	5.73	0.38	1.03
Grayish-white sandstone	0.08	0.53	0.08	3.49	29.25	26.09	3.16	8.26	6.69	1.67	1.03	6.69	1.67	1.03
	0.11	0.84	0.13	5.22	52.43	47.48	4.95	9.59	7.23	1.24	1.18	7.23	1.24	1.18
	0.07	0.48	0.08	3.30	22.87	20.33	2.54	8.00	5.07	2.49	1.35	5.07	2.49	1.35
	0.12	0.83	0.13	6.20	32.61	28.10	4.51	6.23	5.00	1.89	0.89	5.00	1.89	0.89
	0.10	0.68	0.10	5.53	36.49	32.20	4.29	7.51	6.57	1.78	0.95	6.57	1.78	0.95
	0.10	0.72	0.12	5.11	43.41	38.86	4.55	8.54	7.99	1.61	0.88	7.99	1.61	0.88
	0.10	0.75	0.12	5.33	40.09	35.59	4.50	7.91	7.05	1.56	0.86	7.05	1.56	0.86
	0.13	0.87	0.14	7.77	86.07	79.56	6.51	12.22	16.31	1.06	0.77	16.31	1.06	0.77
Gray-greensandstone	0.25	1.61	0.25	14.00	154.71	142.98	11.73	12.19	17.71	0.89	0.69	17.71	0.89	0.69
	0.20	1.30	0.20	16.30	136.66	126.22	10.44	12.09	17.26	0.98	0.83	17.26	0.98	0.83
	0.28	1.90	0.30	14.60	135.49	123.83	11.66	10.62	8.54	0.82	1.33	8.54	0.82	1.33
	0.12	0.90	0.14	5.60	78.07	72.80	5.27	13.81	11.11	0.78	1.42	11.11	0.78	1.42
	0.15	1.03	0.17	6.98	63.27	56.76	6.51	8.72	7.28	1.02	0.99	7.28	1.02	0.99

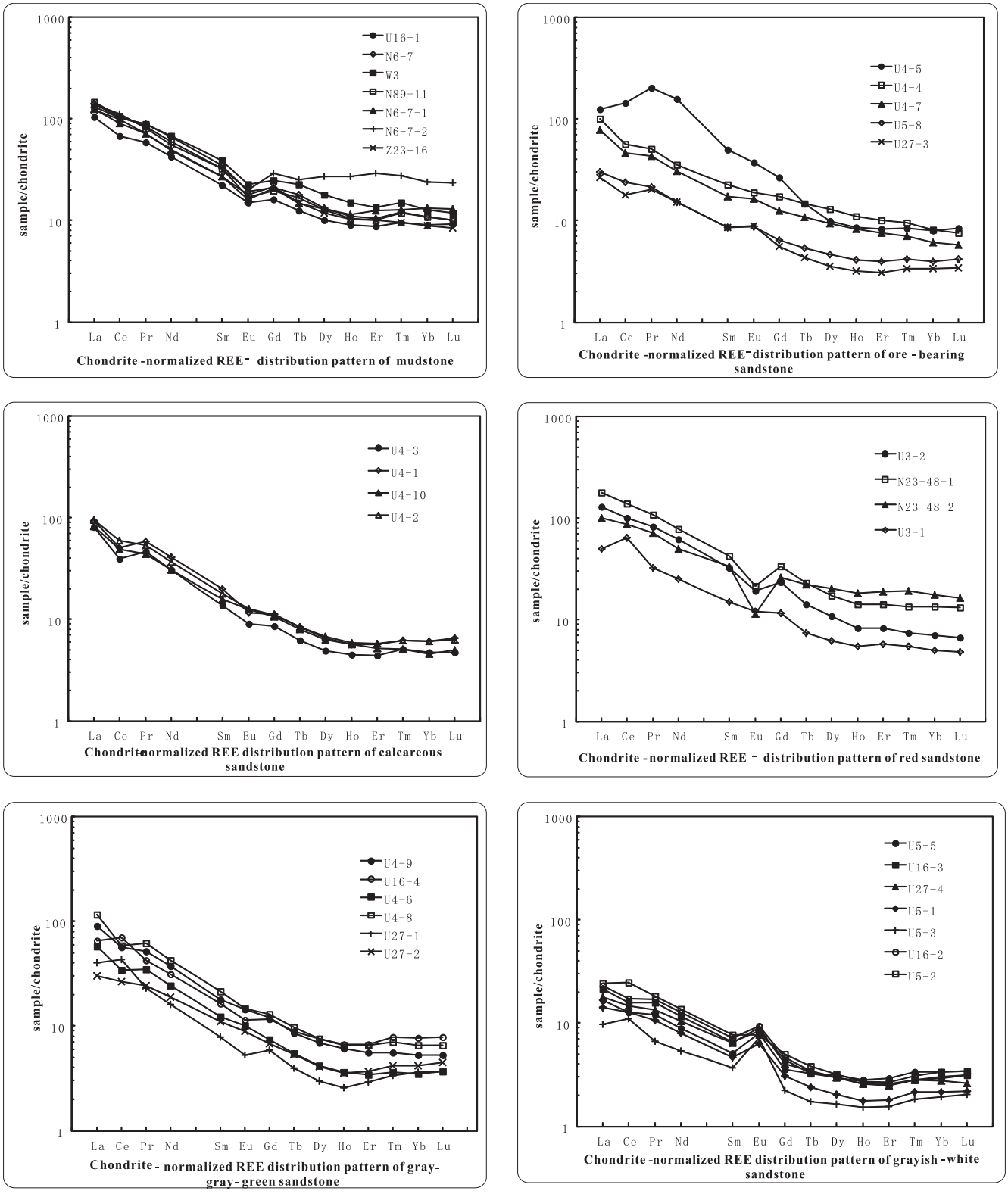

Fig. 10. Chondrite-normalized REE distribution patterns in different sandstones from the Zhiluo Formation in the northern margin of the Ordos Basin.

metallogenic stages. In the Middle Jurassic–Late Cretaceous, with the continuous depletion of oxygen in the fluid and under the influence of the hydrocarbon generation and expulsion in the Yan'an Formation and deeper strata, a dissipation of gaseous reducing agents, such as CH_4 and H_2S, occurred along the fracture in deep oil reservoirs. The coal seam of the Jurassic era is known to be relatively immature (Tuo et al., 2007), and we measured vitrinite reflectance (Ro) to be between 0.4% and 0.57%, confirming this hypothesis. However, numerous kaolinized sandstones and spherical pyrite were discovered at the top of the Yan'an Formation through field outcrops, indicating that the Jurassic coal does generate hydrocarbons. In addition, Jurassic coal is the nearest hydrocarbon to the ore body, and their contribution to mineralization

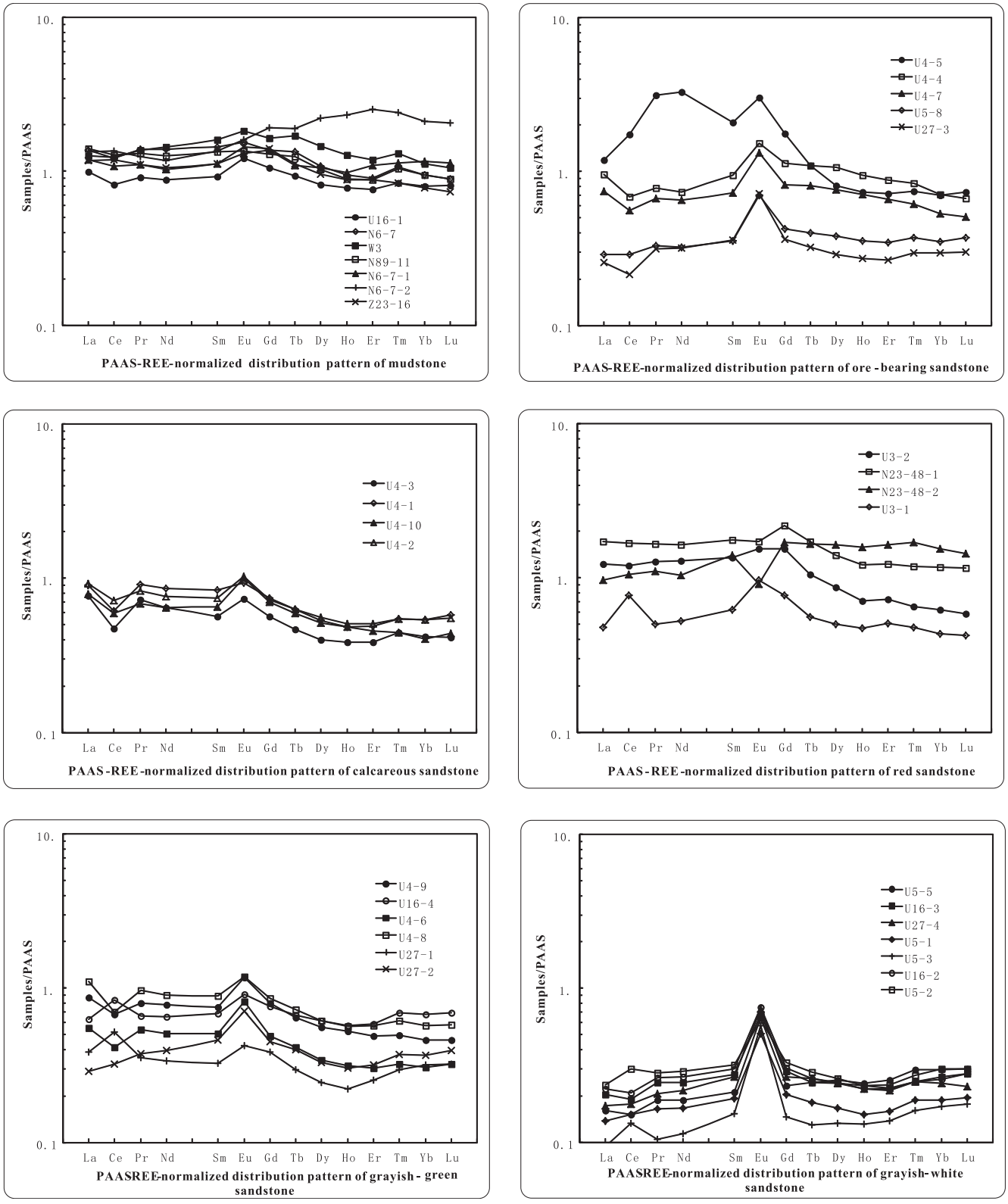

Fig. 11. PAAS-REE-normalized distribution model of different sandstones in the Zhiluo Formation in the northern margin of the Ordos Basin.

should not be underestimated. We agree with previous research that bacteria play an important role in uranium mineralization (Cao et al., 2016). Under the action of anaerobic bacteria, CH_4 reduces the sulfate dissolved in groundwater to H_2S, thus forming the H_2S reducing barrier. When the oxygen- and uranium-bearing water met the reducing fluid, the activated $UO2^{2+}$ uranyl-humic acid complex was reduced to coffinite (Feng et al., 2016). The chemical reaction formula for this reduction is $UO2^{2+} + 2H_2S + Fe^{2+} \rightarrow UO_2 + FeS_2\downarrow + 4H^+$; in this process, feldspar and other easily-soluble minerals experienced further kaolinization. Therefore, the uranium mineralization alteration controlled by the gaseous reductants includes pyritization, carbonation (forming coarse-grained calcite), gypsumization, and reduction-fading

Table 6
The correlation table of rare-earth elements in different types of sandstone, Zhiluo Formation in the northern margin of Ordos Basin.

Rock types	Mudstone	Red sandstone	Gray ore-bearing sandstone	Gray calcareous sandstone	Gray-green sandstone	Grayish-white sandstone
ΣREE(ppm)	221.75	213.18	145.37	126	109.05	36.74
LREE(ppm)	199.65	192.43	133.35	116.5	100.36	32.66
HREE(ppm)	22.1	20.75	12.02	9.5	8.69	4.07
LREE/HREE	9.54	9.83	10.01	11.66	11.61	8

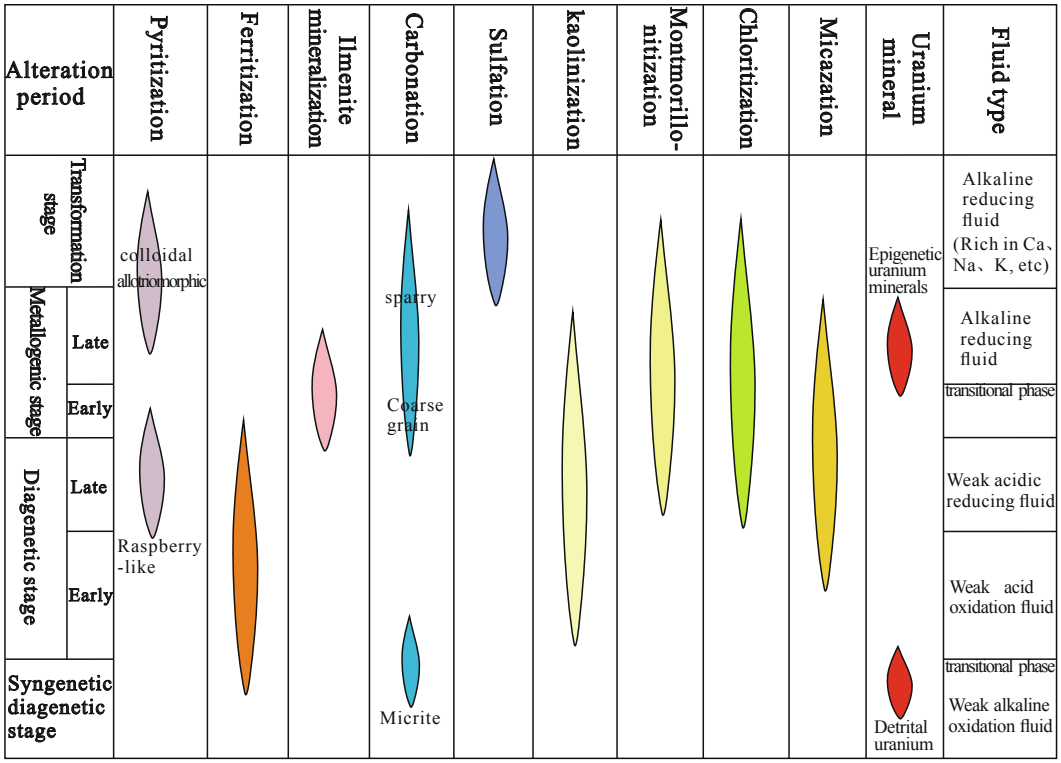

Fig. 12. Generation sequence of altered minerals from the Zhiluo Formation in the northeastern part of the Ordos Basin.

alteration (*i.e.*, grayish–white sandstones). Because of the change in pH value, the rare earths migrated in the form of soluble cations. Simultaneously, the early Yanshan movement exposed the uranium reservoir of the Zhiluo Formation to the surface, resulting in the weathering of kaolinite. Consequently, the REE content in the grayish–white sandstones was significantly reduced. Owing to the overall acidic conditions, carbonate was not stable enough; therefore, coarse-grain calcite mostly underwent dissolution.

During the Early Cretaceous period, the study area experienced the most intense late Yanshan tectonic movement: the stratum reversed and formed a monoclinic structure extending from the southwest to the northeast. Currently, the coal seams of the Jurassic, Permian, and Carboniferous periods as well as the hydrocarbon reservoir of the Triassic period, are located at the maximum buried depth where the hydrocarbon and gas generation capacity of the source rocks reaches a peak (Xue et al., 2010b; Zhang et al., 2016).

6.3. Alkaline reduction fluid phase in the late stage

After Late Cretaceous, the alkaline fluids from the deep part of the strata (mainly oil–gas fluids) further escaped. Consequently, the biotite was chloritized, enriching the fluid in alkaline ions, such as Ca, Na, and K. Therefore, sparry calcite cement and other minerals were formed, whereas uranium mineralization occurred continuously, following this chemical equation: $CH_4 + 4UO^{2+} + 8OH^- \rightarrow 4UO_2 + CO_2 + 6H_2O$.

The Hetao fault depression in the stretch deformation phase of the Himalayas cut off the oxygen- and uranium-bearing water supply channel. Therefore, the role of reduction fluid continued to increase and large-scale gray–green sandstones formed. The reduction fluid protects the stable preservation of later uranium deposits. Additionally, because CO_3^{2-} and REE^{3+} have strong complexing ability, the REE contents in calcareous and ore-bearing sandstones are higher than that in gray–-green sandstones.

Previous studies have shown that the age of the uranium mineralization in the Dongsheng area are Early Cretaceous (124 ± 6 Ma), Late Cretaceous (80 ± 5 Ma), Miocene (20 ± 5 Ma), and Pliocene (8 ± 1 Ma) (Xia et al., 2003; Zhang, 2004; Liu et al., 2007). As the uranium mineralization process continues under the influence of fluids, the Early Cretaceous corresponds to the acidic fluid mineralization stage, and the period after the Late Cretaceous corresponds to the alkaline reductive fluid mineralization stage. With the exhaustion of oxygen and $[UO_2]^{2+}$, the uranium mineralization process gradually entered the reductive fluid preservation stage.

6.4. Mid-low-temperature hydrothermal fluid transformation phase post mineralization

The main metallogenic period of uranium deposits in the study area (80–120 Ma) is the precise period of intense activity of the Yanshanian tectonic–magmatic event in North China (Sun, 1997). Ilmenite, colloidal pyrite, achavalite, sphalerite, and other metal sulfides were found in ore-bearing sandstones via SEM. The geochemical elemental analyses

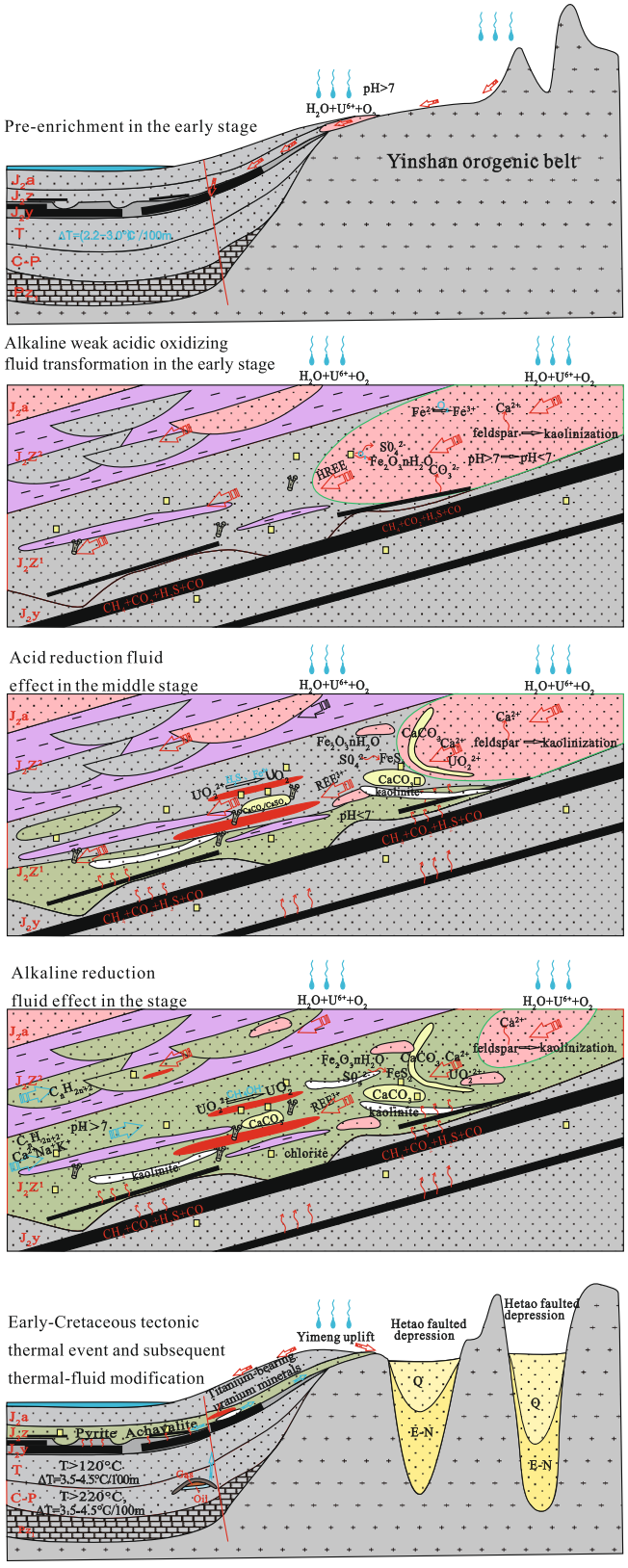

Fig. 13. Schematic diagram of the water-rock reaction stage in the study area.

reveal that the study area has been subjected to the transformation of medium- and low-temperature hydrothermal fluid. Previous studies on the homogenization temperature of fluid inclusions in calcite from ore-bearing sandstones have confirmed that significant tectonic–thermal events occurred in the Ordos Basin after the Middle–Late Jurassic (Xiao et al., 2004b; Cao et al., 2016). These events may have played an important role in activating oil and gas migration, although metallic sulfides, such as colloidal pyrite, selenite, and sphalerite, have been found in the study area. However, does hydrothermal fluid influence the formation of secondary minerals and geochemical changes? Is hydrothermal fluid directly involved in the precipitation and enrichment of uranium, or did it only transform uranium minerals after mineralization? Such questions still have no convincing evidence supporting either hypothesis and more in-depth research is required in this regard.

According to the division of the water-rock reflection stage, the main mineralization stage of sandstone-type uranium deposits began with the weak acid reduction fluid phase in the middle stage and weakened in the alkaline reduction fluid phase in the late stage.

In summary, this study compared the properties of the uranium deposit in the northeastern Ordos Basin with the classic interlayer oxidation zone sandstone-type uranium deposits, and the properties were found to differ in the following three aspects:

(1) The ore-bearing formations of the classic interlayer oxidation zone sandstone-type uranium deposits are mostly primary gray or gray–black sandstones, and a few are variegated sandstones, with the content of organic matter in the ore-bearing sandstone being generally low. For example, the organic matter content in the Syr Darya uranium province in Central Asia ranges between 0.01% and 0.5%. The uranium deposits produced in coal-bearing rock have higher organic matter content; for example, the Kujieertai deposit has an organic matter content ranging between (0.15%–0.8%) (Chen et al., 2003). Minerals that have been altered exhibit obvious zoning. The oxidation zone is characterized by ferroselenium, and the reduction zone is characterized by pyritization, carbonation, and kaolinization. The non-alteration zone is dominated by diagenetic minerals. The ore-bearing formation in the study area contains gray–green and gray sandstones, which are altered types. The organic matter content is relatively high, ranging from 0.07% to 2.66%, with an average of 0.47% (Xue et al., 2009). The types of altered minerals are more diverse, including ferritization, pyritization, ferroselenium, carbonation, sulfation, kaolinization, chloritization, and montmorillonitization.

(2) The sandstones in the oxidation, reduction, and non-alteration zones obviously differ in color and element content in terms of species such as Fe^{3+}, TOC, and S, which can be used to indicate the fluid type. In the study area, the lower component of the Zhiluo Formation mainly comprises gray, gray–green, and gray–white sandstones, whereas the upper component additionally contains a small amount of red sandstones. The color zoning in the plane and vertical direction is not obvious, but using the color is not particularly effective in indicating fluid type.

(3) While uranium minerals in the interlayer oxidation zone sandstone-type uranium deposits are mainly pitchblende, the ore body is roll-type (Li., 2002; Hou et al., 2017). Reductive properties are mainly provided by media such as pyrite and organic carbon in gray sandstones. In the study area, no traditional oxidation–reduction transition zone exists, and uranium minerals are mainly coffinite. The ore bodies are mostly tabular-type produced in gray–green and gray sandstones (Xiang et al., 2006; Zhang et al., 2017; Zhu et al., 2018), and the source of the reducing medium is more complicated; this source includes the acidic fluid provided by the coal seams of the Jurassic, Permian, and Carboniferous periods, and the alkaline fluids from the deep part of the strata (mainly oil–gas fluids). In addition, mineralization may occur during a later event of thermal reformation.

7. Conclusion

(1) Seven types of mineral alterations have been identified in different types of sand bodies of the Zhiluo Formation in the study area

considered herein: ferritization, pyritization, ferroselenium mineralization, carbonation, sulfation, clayization, and uranium mineralization. The variety in alteration types proves that this area has multi-stage fluid mixed mineralization.

(2) Multivariate statistical analyses of the elements in different types of sand bodies in the Zhiluo Formation in the study area were performed. According to the relationship between the main elements and their association, the sandstone components can be classified into three groups. The first is the reduction media group, including CaO, MnO, TOC, S, U, and burning loss. The second is the detrital particle group, including SiO_2, K_2O, and Na_2O. The third contains the clay and volcano component group, including Fe_2O_3, P_2O_5, TiO_2, FeO, MgO, and Al_2O_3. The analysis of the elements reveals the factors influencing uranium enrichment.

(3) The REE of the Zhiluo Formation has a ΣREE value ranging between 22.86 and 355.18 ppm with an average of 137.8 ppm and an LREE/HREE ratio ranging between 5.76 and 18.49 with an average of 10.03. Post chondrite normalization, REE distribution patterns in rocks with different geochemical environments were found to be right-leaning. LaN/YbN (chondrite) ranges from 5 to 18.05 with an average of 11.23. The REE distribution patterns show a fractionation of light and heavy rare earths, a right-leaning enrichment of LREE, and a relatively moderate HREE.

(4) Through PAAS normalization, mudstones of the Zhiluo Formation were found to exhibit a relatively flat curve, whereas sandstones were found to have strong Eu positive anomalies. HREE does not appear to be enriched, whereas HREE and LREE in several types of sandstones are slightly different. We can observe loss of LREE and HREE in grayish–white sandstones. REE characteristics show that although all types of rocks have a similar depositional environment, they underwent oxidation and reduction transformation after the deposition period.

(5) According to the uranium mineralization evolution history in the study area, the water-rock reaction process and mineral-alteration sequence were determined on the basis of alteration types and elemental content. The main mineralization stage of sandstone-type uranium deposits was revealed to have begun with the weak acid reduction fluid phase in the middle stage, and it weakened in the alkaline reduction fluid phase in the late stage.

Acknowledgments

This study was supported by Projects 2015CB453000 of the National Key Basic Research Program (973), the Geological Survey Project of China (DD20160127, DD20190119) and the International Geoscience Program (IGCP, Grant No. IGCP675). The authors thank Ruoshi Jin for his valuable suggestions during the preparation of the manuscript. We also thank the two anonymous reviewers who provided helpful comments and careful reviews of our manuscript.

Appendix A. Supplementary data

Supplementary data to this article can be found online at https://doi.org/10.1016/j.oregeorev.2019.102984.

References

Bonnetti, C., Malartre, F., Huault, V., Cuney, Michel, Bourlange, S., Liu, X.D., Peng, Y.B., 2014. Sedimentology, stratigraphy and palynological occurrences of the late Cretaceous Erlian Formation, Erlian Basin, Inner Mongolia, People's Republic of China. Cretac. Res. 48, 177–192. https://doi.org/10.1016/j.cretres.2013.09.013.

Braum, J.J., Pagel, M., Herbilon, A., Rosin, C., 1993. Mobilization and redistribution of REEs and thorium in a syenitic lateritic profile: a mass balance study. Geochim. Cosmochim. Acta 57, 4419–4434. https://doi.org/10.1016/0016-7037(93)90492-F.

Cao, B.F., Bai, G.P., Zhang, K.X., Zhang, L.K., He, B., 2016. A comprehensive review of hydrocarbons and genetic model of the sandstone-hosted Dongsheng uranium deposit, Ordos Basin, China. Geofluids 16, 624–650. https://doi.org/10.1111/gfl.12182.

Chen, Z.B., Chen, Z.Y., Li, X., 2003. The comparison of metallogenic characteristics between interlayer oxidation zone sandstone type and paleo-valley sandstone type uranium deposit.World. Nucl. Geosci. 20 (1), 1–10 (in Chinese).

Chen, D.S., Wang, R.Y., Li, S.X., 1997. Metallogenic medel of the sandstone-type uranium Deposits in interlayer oxidation zone of YiLi Basin. Uranium Geol. 13 (6), 327–335 (in Chinese with English abstract).

Chen, Y.L., Zhu, X.Y., Zhang, C.J., Chen, Y.H., Peng, X.J., Wang, J.P., 2007. A Preliminary study on REE transformation regularities of the interlayer oxidation zone in sandstone-type uranium deposit: In case of the Ili and Turpan-Hami Basins. Geol. Rev. 53 (4), 473–485 (in Chinese with English abstract).

Cheng, Y.H., Wang, S.Y., Li, Y., Ao, C., Li, Y.F., Li, J.G., Li, H.L., Zhang, T.F., 2018. Late Cretaceous-Cenozoic thermochronology in the southern Songliao Basin, NE China: New insights from apatite and zircon fission track analysis. J. Asian Earth Sci. 160, 96–106. https://doi.org/10.1016/j.jseaes.2018.04.015.

Cheng, Y.H., Wang, S.Y., Jin, R.S., Li, J.G., Ao, C., Teng, X.M., 2019. Global Miocene tectonics and regional sandstone-style uranium mineralization. Ore Geol. Rev. 106, 238–250. https://doi.org/10.1016/j.oregeorev.2019.02.003.

Darby, B.J., Davis, G.A., Zheng, Y., 2001. Structural evolution of the southwestern Daqing Shan, Yinshan belt, Inner Mongoli, China. Memoir Geol. Soc. Am. 194, 199–214.

Davis, G.A., Zheng, Y., Wang, C., Darby, B.J., Zhang, C.H., Gehrels, G., 2002. Mesozoic tectonic evolution of the Yanshan fold and thrust belt with emphasis on Hebei and Liaoning provinces, northern China. Beijing Geol. 194, 171–197. https://doi.org/10.1130/0-8137-1194-0.171.

Deng, J., Wang, Q.F., Gao, B.F., Huang, D.H., Yang, L.Q., Xu, H., Zhou, Y.H., 2005b. Evolution of Ordos Basin and its distribution of various energy resources. Geoscience 19 (4), 538–545 (in Chinese with English abstract).

Deng, J., Wang, Q.F., Huang, D.H., Gao, B.F., Yang, L.Q., Xu, H., 2005a. Basement evolution of the Ordos Basin and its constraint on cap rock. Earth Sci. Front. (China University of Geoscience, Beijing, Peking University) 12 (3), 91–99 (in Chinese with English abstract).

Feng, Z., Nie, F., Yan, Z., Jiang, L., Gu, S., Chen, L., 2014. Structure and fluid evolution of the western slope of Songliao Basin and its relation to sandstone type uranium mineralization. J. East China Inst. Technol. (Nat. Sci.) 37 (1), 13–20 (in Chinese with English abstract).

Feng, Q., Qin, Y., Fu, S.T., Liu, Y.Q., Zhou, D.W., 2016. The enrichment of calcite and the genesis of uranium deposits in Dongsheng uranium sandstone. Geol. J. China Univers. 22 (1), 53–59 (in Chinese with English abstract).

Fleet, A.J., 1984. Chapter10-Aqueous and sedimentary geochemistry of the rare elements. Dev. Geochem. 2, 343–373. https://doi.org/10.1016/B978-0-444-42148-7.50015-0.

Han, X.Z., Zhang, Z.L., Yao, C.L., Li, S.X., Miao, A.S., Yang, J.X., 2009. Structual characteristic and its control to uranium mineralization in the Northeast of Ordos Basin. Uranium Geol. 25 (4), 277–283 (in Chinese with English abstract).

Henderson, P., ed., Tian, S.F., Shi, L., translate.1984.Rare earth element geochemistry. Geology publishing house. 213.

Hou, B.H., Keeling, J., Li, Z.Y., 2017. Paleovalley-related uranium deposits in Australia and China: a review of geological and exploration models and methods. Ore Geol. Rev. 88, 201–234. https://doi.org/10.1016/j.oregeorev.2017.05.005.

Huang, S.J., Huang, K.K., Feng, W.L., Tong, H.P., Liu, L.H., Zhang, X.H., 2009. Mass exchange among feldspar, kaolinite and illite and their influences on secondary porosity formation in clastic diagenesis-a case study on the Upper Paleozoic Ordos Basin and Xujiahe Formation, Western Sichuan Depression. Geochimica 38 (5), 498–506 (in Chinese with English abstract).

Huang, J.B., Li, S.X., 2007. Metallogenic characteristics, model and exploration prospect for the paleo-interlayer-oxidation type sandstone-hosted uranium deposits in China. Uranium Geol. 23 (1), 7–16 (in Chinese with English abstract).

Huang, C.M., Wang, C.S., 2002. Geochemical features of rare earth elements in process of rock weathering and soil formation. Chin. Rare Earths 23 (5), 46–49 (in Chinese with English abstract).

Jiao, Y.Q., Lu, X.B., Wang, Z.H., Wang, M.F., 2004. Two distinct geological environments from dedimentary to diagenesis stages: examples from sandstone-type uranium deposits, Turpan-Hami Basin. Earth Sci. –J. China Univ. Geosci. 29 (5), 615–620 (in Chinese with English abstract).

Jiao, Y.Q., Chen, A.P., Yang, Q., Peng, Y.B., Wu, L.Q., Miao, A.S., Wang, M.F., Xu, Z.C., 2005. Sand body heterogeneity: one of the key factors of uranium metal logenesis in Ordos Basin. Uranium Geol. 21 (1), 8–16 (in Chinese with English abstract).

Jiao, Y.Q., Wu, L.Q., Rong, H., Peng, Y.B., Wan, J.W., Miao, A.S., 2012. Uranium reservoir architecture and ore-forming flow field study: a key of revealing dongsheng sandstone-type uranium deposit mineralization mechanism. Geol. Sci. Technol. Inf. 32 (5), 94–104 (in Chinese with English abstract).

Jin, R.S., Miao, P.S., Sima, X.Z., Feng, X.X., Tang, C., Zhu, Q., Li, G.Y., 2014b. Discussion on the classification about the uranium deposits. Geol. Surv. Res. 37 (1), 1–5 (in Chinese with English abstract).

Jin, R.S., Zhang, C.J., Feng, X.X., Tang, C., Zhu, Q., Li, G.Y., 2014a. The influence of fluid mixing on the mineralization of sandstone type uranium deposits. Geol. Bull. China 33 (2/3), 354–358 (in Chinese with English abstract).

Jin, R.S., Cheng, Y.H., Yang, J., Ao, C., Li, J.G., Li, Y.F., Zhou, X.X., 2016. Classification and correlation of Jurassic uranium-bearing series in the Junggar Basin. Acta Geol. Sin. 90 (12), 3293–3309 (in Chinese with English abstract).

Kovačević, J., Nikić, Z., Papić, P., 2009. Genetic model of uranium mineralization in the Permo-Triassic sedimentary rocks of the Stara Planina eastern Serbia. Sed. Geol. 219 (1), 252–261. https://doi.org/10.1016/j.sedgeo.2009.05.015.

Li, T., 1994. Element abundances of China's continental crust and its sedimentary layer and upper continental crust. Geochimica 23 (2), 140–145 (in Chinese with English abstract).

Li, 2002. Characteristics of sandstone-type uranium mineralization and ore-controlling factors in Wukurqi ore district at southern margin of Yili Basin, Xinjiang. Uranium

Geol. 18 (1), 28–35 (in Chinese with English abstract).
Li, Z.Y., Chen, A.P., Fang, X.H., Ou, G.X., Xia, Y.L., Sun, Y., 2008. Origin and superposition metallogenic model of the sandstone-type uranium deposit in the northeastern Ordos Basin, China. Acta Geol. Sin. 82 (4), 745–749 (in Chinese with English abstract).
Li, R.X., Li, Y.Z., 2011. The geologic features of mineralization at the Dongsheng uranium deposit in the northern Ordos Basin(Central China). Russ. Geol. Geophys. 52, 593–602. https://doi.org/10.1016/j.rgg.2011.05003.
Liu, W.J., 1991. Application of common data of sedimentary geochemistry. ShanXI Geol. 6 (1), 109–123 (in Chinese with English abstract).
Liu, X.W., Cheng, K.M., 1995. Application of trace element in the study of petroleum from coals. Petrol. Explor. Dev. 22 (5), 40–44 (in Chinese with English abstract).
Liu, H.B., Xia, Y.L., Tian, S.F., 2007. Study on geochronology anduranium source of sandstone type uranium deposit in Dongsheng area. Uranium Geol. 23 (1), 23–29 (In Chinese with English abstract).
Liu, W.Y., Xiao, L.P., Liang, B., 2008. Study on the treatment of acid mine drainage by SAPS and the development prospect of SAPS. Min. R&D 28 (1), 71–73 (in Chinese with English abstract).
Lu, H.B., Jiang, Z.X., 1999. Application of geochemical analysis of rare earth elements in the study of lithofacies paleogeography. J. Univ. Petrol., China 23 (1), 6–8 (in Chinese with English abstract).
Luo, J.L., Liu, X.H., Zhang, F.X., Jia, H., Li, B., 2005. Petrology and diagenesis of uranium-bearing sandstones in Dongsheng area of Ordos Basin and Shihongtan area of Tuha Basin. Acta Petrol. Sin. 26 (4), 39–49 (in Chinese with English abstract).
McLennan, S.M., 1989. Rare earth elements in sedimentary rocks: influence of provenance and sedimentary processes. Rev. Mineral. 21, 169–200.
Michard, A., 1989. Rare earth element systematics in hydrothermal fluids. Geochim. Cosmochim. Acta 53, 745–750.
Min, M.Z., Xu, H.F., Chen, J., Fayek, Mostafa, 2005. Evidence of uranium in sandstone-hosted roll-front uranium deposits, northwestern China. Ore Geol. Rev. 26, 198–206. https://doi.org/10.1016/j.oregeorev.2004.10.003.
Nesbitt, H.W., Young, G.M., 1984. Prodication of some weathering trends of plutonic and vocanic rocks based on thermodynamic and linetic considerations. Geochim. Acta 48, 1523–1534. https://doi.org/10.1016/0016-7037(84)90408-3.
Pan, A.F., Li, R.J., He, Y., 2007. Geochemical characteristics of elements in the Dongsheng uranium deposit, Ordos Basin. J. Northwest Univ. (Natural Science Edition) 37 (2), 291–296 (in Chinese with English abstract).
Pan, J.Y., Liu, C.D., Guo, G.L., Chen, A.P., Chen, F.Z., Yan, Z.B., Chen, Y.P., Wu, R.G., 2009. The discovery of selenium-bearing minerals in the Tamusu sandstone-type uranium deposits, Inner Mongolia, China and its significance. Acta Mineral. Sin. 29 (1), 44–48 (in Chinese with English abstract).
Peng, Y.B., Li, Z.Y., Fang, X.H., Xie, Q.L., 2006. Metallogenetic characteristics of NO.2081 uranium deposit in the North of Ordos Basin. Acta Mineral. Sin. 26 (3), 349–355 (in Chinese with English abstract).
Price, R.C., Gray, C.M., Wilson, R.E., Frey, F.A., Taylor, S.R., 1991. The effect of weathering on rare earth element, Y and Ba abundances in Tertiary basalts from southeastern Australia. Chem. Geol. 93, 245–265. https://doi.org/10.1016/0009-2541(91)90117-A.
Quan, Z.G., Li, Z.S., 2002. Geological characteristics and genesis of the Shihogntan sandstone-type uranium deposit, Xinjiang. Gelol. Rev. 43 (6), 430–436 (in Chinese with English abstract).
Rollison, H.R., 1993. Using Geochemical Date: Evaluation, Presentations, Interpretation. Longm and Scientific Technical Press, London, pp. 106–111.
Rollison, H.R., ed., Yang,X.M.,Yang, X.Y.,Chen, S.X., translate. 2000. Rock geochemistry. University of Science and Technology of China Press, pp.116-117.
Shao, L., Liu, Z.W., Zhu, W.L., 2000. Application of sedimentary geochemistry of terrigenous clastic rock to basin analysis. Earth Sci. Front. (China University of Geosciences, Beijing) 7 (3), 297–304 (in Chinese with English abstract).
Sun, S.H., 1997. Study on tectonic thermal events in Ordos Basin. Chin. Sci. Bull. 42 (3), 306–309 (in Chinese with English abstract).
Tang, C., SiMa, X.Z., Zhu, Q., Feng, X.X., Chen, Y., Chen, L.L., Liu, X.X., 2016. Carbon and oxygen isotopic composition and uranium mineralization significance of calcite of Zhiluo Formation uranium-earing sandstones in Dongsheng area. Geol. J. China Univ. 22 (4), 698–706 (in Chinese with English abstract).
Taylor, S.R., Mclennan, S.M., 1985. The Continental Crust: Its Composition and Evolution. Blackwell Scientific Publications, Oxford, UK, pp. 1–372.
Tu, G.Z., 1998. Cryogenic Geochemistry. Science Press, Beijing, pp. 93–106 (in Chinese).
Tuo, J.C., Ma, W.Y., Zhang, M.F., Wang, X.B., 2007. Organic Geochemistry of the Dongsheng sedimentary uranium ore deposits, China. Appl. Geochem. 22, 1949–1969.
Wang, J.P., 2006. Preliminary study on the existence characteristics of rare earth elements in the interstratified oxidized zone. In: China Nuclear Science and Technology Report, pp. 200–209 (in Chinese with English abstract).
Wang, Z.L., Liu, C.Q., Xu, Z.F., Han, G.L., Zhu, J.M., Zhang, Jin, 2000. Advances in research on geochemistry of rare earth elements in rivers. Adv. Earth Sci. 15 (5), 553–558 (in Chinese with English abstract).
Wang, Q.Z., Pan, J.Y., Cao, S.L., Guan, T.Y., Zhang, G.Y., 2006. Super-enriching mechanism of disperse-elements Re and Se in interlayer oxidation-A case study of the Zhajistan interlayer oxidation zone sandstone-type uranium deposit, Ili Basin, Xinjiang. Geol. Rev. 52 (3), 358–362 (in Chinese with English abstract).
Wang, Z.G., Yu, X.Y., Zhao, Z.H., 1989. Earth Chemistry of Rare Earth Elements. Science press.
Wei, S.Y., Qin, M.K., Li, Y.X., He, Z.B., Chen, A.P., Shen, K.F., Cao, J.Y., 2006. Tectono sedimentary evolution of Erlian Basin since Late Mesozoic and sandstone～hosted uranium metallogenesis. Uranium Geol. 22 (2), 76–82 (in Chinese with English abstract).
Wu, Z.J., Han, X.Z., Yi, C., Qi, C.J., Hui, X.C., Wang, M.T., 2013. Geochemistry of sandstones from the Middle Jurassic Zhiluo Formation, Dongsheng district, northeastern Ordos Basin: implication for Provenance and Tectonic setting. Geoscience 27 (3), 557–567 (in Chinese with English abstract).
Wu, B.L., Huang, Z.Z., Li, X.Z., Zhang, F., 2003. Initial discussion on paleo fluid geologic process and sandstone type uranium metallogenesis at southwestern edge of Turpan-Hami Basin. Uranium Geol. 19 (6), 326–332 (in Chinese with English abstract).
Wu, B.L., Liu, C.Y., Zhang, F.X., Fang, X.H., Liu, X., 2006. Geochemical characteristics of epigenetic alteration in Dongsheng sandstone-type uranium deposit and its metal logenic dignification. Acta Geol. Sin. 80 (5), 740–747. https://doi.org/10.1007/s11631-007-0235-z.
Wu, B.L., Zhang, W.Y., Song, Z.S., Cun, X.N., Sun, L., Luo, J.J., Li, Y.Q., Cheng, X.H., Sun, B., 2016. Geological and geochemical characteristics of uranium minerals in the sandstone-type uranium deposits in the north of Ordos Basin and their genetic significance. Acta Geol. Sin. 90 (12), 3393–3407 (in Chinese with English abstract).
Xia, Y.L., Lin, J.R., Liu, H.B., Fan, G., Hou, Y., 2003. Research on geochronology and sandstone-hosted uranium ore formation inmajor uranium productive basins, northern China. Uranium Geol. 19 (3), 129–136 (In Chinese with English abstract).
Xiang, W.D., Fang, X.H., Li, T.G., Chen, X.L., Pang, Y.Q., Cheng, H.H., 2006. Metal logenic characteristics and model of Dongsheng uranium deposit in Ordos Basin, North China. Uranium Geol. 22 (5), 257–266 (in Chinese with English abstract).
Xiao, X.J., Li, Z.Y., Fang, X.H., Ou, G.X., Sun, Y., Chen, A.P., 2004b. The evidences and significances of epithermal mineralization fluid in the Dongsheng sandstone type uranium deposit. Bull. Mineral. Petrol. Geochem. 23 (4), 301–304 (in Chinese with English abstract).
Xiao, X.J., Li, Z.Y., Chen, A.P., 2004a. Prel iminary study on features of mineralogical zoning of epigenetic alteration at sandstone-type uranium deposit, Dongsheng area, Ordos Basin. Uranium Geol. 20 (3), 136–140 (in Chinese with English abstract).
Xue, C.J., Chi, G.X., Xue, W., 2010a. Interaction of two fluid systems in the formation of sandstone-hosted uranium deposits in the Ordos Basin: geochemical evidence and hydrodynamic modeling. J. Geochem. Explor. 106, 226–235. https://doi.org/10.1016/j.gexplo. 2009.11.006.
Xue, H., Zhang, J.C., Xu, B., Wang, Y., Mao, X.P., 2010b. Evaluation of Upper Paleozoic source rocks of the Hangjinqi block in the northern Ordos Basin, China. J. Chengdu Univ. Tech. 37 (1), 21–28 (in Chinese with English abstract).
Xue, W., Xue, C.J., Chi, G.X., Tu, Q.J., Kang, M., Gao, Y.L., 2009. Some relations of uranium mineralization and organic matter in Jurassic strata on the northeastern margin of Ordos Basin, China. Geol Rev. 55 (3), 361–369.
Yang, S.Y., Li, C.X., 1999. Research progress in REE tracer for sediment source. Adv. Earth Sci. 14 (2), 164–167 (in Chinese with English abstract).
Yang, X.Y., Luo, X.D., Ling, M.X., Lai, X.D., 2008. Geochemical features of sandstone-type uranium deposits in the Ordos Basin and their geological significances. Geol Rev. 54 (4), 539–549 (in Chinese with English abstract).
Zhang, R.L., 2004. Uranium metallogenic conditions and prospecting direction in Jiulongzhang volcanic Basin. Uranium Geol. 20 (4), 213–218 (in Chinese with English abstract).
Zhang, L., Liu, C.Y., Zhao, Z.P., Wang, F.F., Song, Z.S., 2015a. Fluid evolution and mineralization of Hangjinqi sandstone-type uranium deposit, Ordos Basin. Earth Sci. Front. 22 (3), 368–381 (in Chinese with English abstract).
Zhang, L., Liu, C.Y., Fayek, M., Wu, B.L., Lei, K.Y., Cun, X.N., Sun, L., 2017. Hydrothermal mineralization in the sandstone-hosted Hangjinqi uranium deposit, north Ordos Basin, China. Ore Geol. Rev. 80, 103–115. https://doi.org/10.1016/j.oregeorev.2016.06.012.
Zhang, G.X., Miao, A.S., Li, W.H., Guo, H.K., 2016. The role of boerjianghaizi faults in sandstone-type uranium mineralization. J. East China Univ. Technol. (Natural Science) 39 (1), 15–22 (in Chinese with English abstract).
Zhang, C.Y., Nie, F.J., Hou, S.R., Deng, W., Wang, J.L., Zhang, L., 2015b. Study on hydrothermal alteration and relation with uranium mineralization of the Tamusu exogenetic uranium deposit, Inner Mongolia, China. Acta Mineral. Sin. 35 (1), 80–86 (in Chinese with English abstract).
Zhang, F.X., Qiao, H.M., Jia, H., 2006. The metallogenic condition and epigenetic alteration mineralization of Dongsheng uranium deposit in the Inner Mongolia. Acta Geol. Sin. 80 (5), 733–739 (in Chinese with English abstract).
Zhang, J.D., Xu, G.Z., Chen, A.P., Wang, C., 2005. Preliminary discussion on uranium metallogenic models of China's insitu leachable sandstone-type uranium deposits. Uranium Geol. 21 (3), 139–145 (in Chinese with English abstract).
Zhao, H.L., Chen, L.L., Feng, X.X., Li, J.G., Chen, Y.Y., Wang, G., 2018. Features of clay minerals in the Middle Jurassic Zhiluo Formation sandstones of the Nalinggou area in the Ordos Basin and a preliminary comparison with adjacent area. Geol. J. China Univ. 24 (5), 627–636 (in Chinese with English abstract).
Zhao, C.L., Zhu, X.M., 2001. Sedimentary Petrology. Petroleum Industry Press (in Chinese with English abstract).
Zheng, M.L., Jin, Z.J., Wang, Y., Liu, C.Y., Xu, G.Z., 2006. Structural characteristics and evolution of north Ordos Basin in Late Mesozoic and Cenozoic. J. Earth Sci. Environ. 28 (3), 31–36 (in Chinese with English abstract).
Zhu, Q., Li, J.G., Yu, R.A., Sima, X.Z., Wen, S.B., Li, G.Y., Si, Q.H., 2018. Lithologic-lithographic characteristics of the Upper and Lower Members of the Zhiluo Formation and their differential control of uranium mineralization in the Tarangaole area, Ordos Basin (in Chinese with English abstract). Acta Geosci. Sin. http://kns.cnki.net/kcms/detail/11.3474.P.20180905.1418.002.html.
Zhu, X.Y., Wang, Y.L., Wang, Z.C., Zhang, C.J., Liu, J.H., 2003. Trace element geochemistry of sandstone-type uranium deposits in Dongsheng area. Geol. Geochem. 31 (2), 30–45 (in Chinese with English abstract).